Molecular Simulation of Adsorption at Solid-Aqueous Interfaces

by

Travis Gerard Trudeau
B.Sc., Thompson Rivers University, 2006
Dipl. Journalism, Thompson Rivers University, 2008

A thesis submitted in Partial Fulfillment of the
Requirements for the Degree of

MASTER OF SCIENCE

in the Department of Chemistry

Molecular Simulation of Adsorption at Solid-Aqueous Interfaces

by

Travis Gerard Trudeau
B.Sc., Thompson Rivers University, 2006
Dipl. Journalism, Thompson Rivers University, 2008

Supervisory Committee

Dr. Dennis K. Hore, Supervisor
(Department of Chemistry)

Dr. Irina Paci, Departmental Member
(Department of Chemistry)

Dr. Alexandre G. Brolo, Departmental Member
(Department of Chemistry)

Supervisory Committee

Dr. Dennis K. Hore, Supervisor
(Department of Chemistry)

Dr. Irina Paci, Departmental Member
(Department of Chemistry)

Dr. Alexandre G. Brolo, Departmental Member
(Department of Chemistry)

ABSTRACT

The structure of liquid water and adsorbed leucine at solid surfaces of tunable hydrophobicity has been examined by molecular dynamics simulation. The results have been used to extend models of water ordering at superhydrophobic surfaces to create a general model of density-dependent ordering of water and adsorbates at hydrophobic interfaces. In this model, interfacial water structures can be classified according to two hydrophobic regimes, a non-wetting structure and a semi-wetting structure, distinguished by the orientation of interfacial water molecules. We propose that the emergence of the wetting-type order is strongly dependent on the density profile across the interfacial region. Leucine adsorbed at the same surfaces also shows two patterns of adsorption, distinguished by the proportion of time the molecule adopts an orientation parallel to the surface. These patterns correspond to the non-wetting and semi-wetting regimes of water and also arise from the density structure of water in the interfacial region.

Contents

List of Tables

List of Figures

ACKNOWLEDGEMENTS

I would like to thank:

My brother Michael, who remains the wisest man I know.

Dennis Hore, my advisor, for his guidance and boundless enthusiasm.

Shaun Hall, for his encouragement and insight, and for introducing me to Invader Zim.

Kailash Jena, for our discussions about sum frequency generation.

NSERC, for financial support.

The University of Victoria, for its financial support.

Even the longest journey must begin where you stand.

Lao Tzu

Chapter 1

Introduction

1.1 Water Structure at Solid Surfaces

The equilibrium structure of water near solid interfaces is of interest for several reasons. First, as water is the most important and most widely studied solvent in existence, studies of its behaviour are naturally intriguing. Second, solvents in general [1, 2] and water in particular [3, 4] are increasingly seen as important factors in the adsorption of solutes on solid surfaces (Figure 1.1. More than other solvents, water has the potential to be an active agent in adsorption of solutes because of the strong interactions between water molecules, which give rise to the hydrophobic effect [5] and hydration forces, as are depicted in Figure 1.2. The effect of adsorbates in disrupting water-water interactions at the interface may be as important to adsorption as the formation of water-solute solvation interactions or the interactive force between surface and solute. It is impossible to gauge the effect of this disruption without understanding the structure of water in the absence of any solute. Strong ordering may repel an incoming solute, or a solute may adsorb to a surface indirectly, by interacting with one or more layers of highly-ordered water at the interface.

Interfacial chemistry in general has only begun to yield to analysis in recent decades, and experiment remains limited in several crucial respects. The central difficulty in studying interfacial chemistry is that although the interfacial region may be responsible for much of the chemical and physical properties of a system, it represents only a tiny fraction of the system itself. Interfacial signals tend to be overwhelmed by signals from

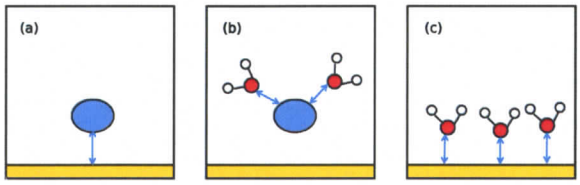

Figure 1.1: Adsorption of a solute is governed by the interactions of (a) solute and surface, (b) solute and solvent (through solvation at the surface), and (c) surface and solvent (through effects such as hydrophobic attraction and hydration repulsion)

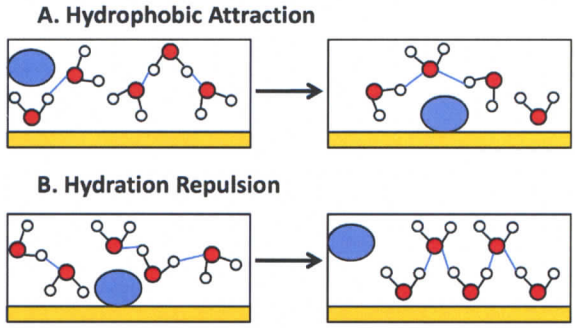

Figure 1.2: Interaction between surface and solvent is important in controlling adsorption of a solute. Weak surface-solvent interactions will favor solute adsorption (hydrophobic attraction), while strong surface-solvent interactions will tend to repel incoming solute (hydration repulstion).

the bulk [6]. Over the past few decades a handful of techniques have emerged which can at least in part overcome this limitation, and have proven especially useful for characterizating water structure at solid surfaces: X-ray diffraction [7], neutron scattering [8], surface enhanced Raman spectroscopy [9], and even-order nonlinear techniques such as second-harmonic [10–12] and sum-frequency generation (SFG) [6, 13–17] spectroscopy.

These techniques have achieved some success, but current experiment has two crucial limitations which can be addressed by simulation work. First, experiments provide only very coarse resolution of the interfacial water structure. Any interface-specific method will necessarily pick up signals from regions across the interface, both immediately adjacent to the surface and farther away from it. These regions may be ordered in very different ways, and there is no method of distinguishing signals from different parts of the interface.

Signals will also be returned from different parts of the surface; a completely isotropic surface is a practical impossibility, and surface features or different faces of a surface can order water in different ways. Experimental techniques will capture signals from a broad region of the non-isotropic surface. The result is a throroughly blended signal obtained from what are effectively many different surface environments.

In addition, the results of experiment require judgment and interpretation which can be open to debate. Questions as simple as what groups are involved in adsorption of an amino acid can have several possible answers [18].

In contrast to experiment, molecular dynamics simulations can provide pictures of the interface which are complete to atomic and picosecond detail. They also provide information which does not require interpretation; the structure of water in an MD simulation needs only to be analyzed and explained. Computers can never replace laboratories. However, because they are complete and unambiguous, simulations can provide a valuable tool in explaining the results of experiments. They can also illuminate phenomena which have not yet been observed, providing direction and impetus for future experiments.

1.1.1 A Note Regarding Terminology

The terms 'hydrophobic,' 'hydrophilic', 'wetting', and 'nonwetting' have been used with different exact definitions in the past. In the current paper, we use 'hydrophobic' to connote a non-polar surface, and 'hydrophilic' to mean a polar one. The theoretical surfaces we studied were all nonpolar, and thus are consistently refered to as 'hydrophobic', while surfaces in related experiments may be termed either 'hydrophobic' or 'hydrophilic.' We avoid defining surfaces as either strictly 'wetting' or 'nonwetting,' although the cutoff between these is usually considered to be at a contact angle of 90°. Instead, we refer to surfaces' wettability relative to one another; our 'nonwetting' surfaces are simply those we measured with the highest contact angles.

1.2 Amino Acid Adsorption at Solid Surfaces

Amino acids are arguably the most important biological molecules in existence. They are the monomeric units of proteins, which perform almost all of the catalytic [19, 20] and many of the structural functions [21, 22] of cells, as well as playing a crucial role in the immune system as the primary components of antibodies [23].

Despite their diverse functions within proteins, amino acids themselves are quite simple. As their name implies, each consists of an amine group and a carboxylic acid group, joined by a single carbon atom. In nineteen of the twenty common amino acids, the central carbon is chiral, possessing an organic side chain which gives each amino acid its distinct chemical properties. Proteins and polypeptides are extended sequences of amino acids joined by special amide bonds called peptide bonds which form between the amine and carboxyl groups of amino acids by dehydration reaction. In the absence of a peptide bond, all amino acids will exist at some pH as a zwitterion, with positive and negative formal charges in their structure but an overall charge of zero. A non-basic, non-acidic amino acid will be zwitterionic at pH values around 7, with its protonated amine carrying a positive charge and its deprotonated carboxyl carrying a negative charge.

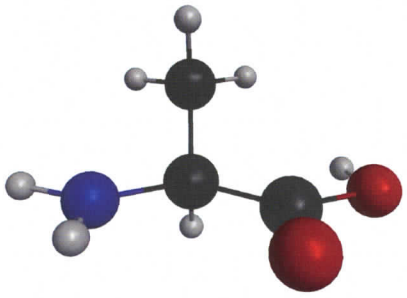

Figure 1.3: Alanine has a methyl group as a side chain and is the simplest amino acid to possess chirality. Virtually all chiral amino acids exist in the L-conformation depicted here.

Many of the properties of proteins can be inferred from the sequence of their individual amino acids [24,25]. Amino acids with similar side chains tend to exhibit similar properties and often have a similar effect on overall protein function. For this reason, amino acids are grouped into several categories depending on their side chain identity. Basic and acidic amino acids have additional amine or carboxyl groups on their side chains, and are often charged at pH values near neutrality. Polar amino acids have alcohol or amide groups and are hydrophilic. Nonpolar amino acids have aromatic or aliphatic hydrocarbon side chains. A few other amino acids have unique properties, such as cysteine and tryptophan, and tend to be involved in highly specific interactions, such as the formation of sulfide bonds between cysteine units to link different regions of a protein together.

Nonpolar amino acids are the major constituents of most proteins, making up more than 70% of amino acids in modern proteins [26]. Because of their hydrophobic properties, they are often found in the interiors of proteins in aqueous solution, shielded from interactions with water.

All twenty of the most-common amino acids are required for survival in human beings. Seven of these are generally considered 'indispensable' since they cannot be synthesized by human metabolism and must be ingested. The other thirteen amino acids can be considered 'conditionally indispensable', since their rates of synthesis are limited by supply

of precursors and natural processes; a diet severely deficient in any of the animo acids is likely to have negative health consequences [27]. Given this, it is not surprising that the largest commercial uses of amino acids involve their consumption as food, as flavouring agents and as an additive to feed stock [28]. Depending on the amino acid desired and its application, there are a variety of methods of synthesizing amino acids or extracting them from natural products. Regardless of their origin, however, all amino acid sources require separation techniques to obtain a desired product in significant purity [29]. This has lead to a signficant body of literature regarding chromatography of amino acids [30–35]. The rapid and efficient separation of amino acids remains a major goal of industrial chemistry in this field. Future applications of chormatographic technology may include the binding of amino and carboxyl groups to columns for separatory [36] or biofunctional [37] purposes. Proteins adsorbed on stationary hydrophobic phases have been found to be kinetically stable and resistant to displacement by other proteins [38], raising the possibility of rapidly pretreating columns for a variety of functions.

Some natural phenomenon involve the same principles as chromatography, such as the partitioning of organic waste to soil particles [39], or desired amino acid products to adsorbents [40] and these are of interest to those who study amino acid adsorption as well.

The chirality of all amino acids (except glycine, which has a hydrogen atom for a side chain) is an important feature. Virtually all amino acids in biological systems are of the L-conformation [26, 41] (S absolute conformation) depicted in Figure 1.3, although there are rare examples of naturally expressed D-amino acids [42]. Since both absolute conformations are of equal stability and are formed in equal amounts under normal conditions from non-chiral starting materials, the origin of this imbalance is a subject of considerable interest, and probably arose early in or even before the origin of life [43].

In hypotheses about the origin of amino acid chirality, adsorption on solid surfaces often plays a major role [26, 41, 43]. According to these models, differential adsorption of enantiomers of some amino acids may have lead to the initial discrepancy between L- and

R- amino acids which persists in a much more extreme form to this day. The theory of clay adsorption is most popular among the 'concentrating' theories [43], which hold that life arose in a microenvironment in which the materials of life, such as amino acids, were concentrated relative to the surrounding dilute prebiotic solution. One major advantage clay adsorption has over competing 'concentrating' models such as those centered on micelle microenvironments is that certain clay surfaces have shown catalytic activity including peptide bond formation [44].

Zaia [26] noted that most experiments which tested differential adsorption of amino acids on solid surfaces were conducted with polar surfaces that preferentially adsorbed positively or negatively charged amino acids, leading to a large concentration of these amino acids. Almost three-quarters of amino acids in modern proteins, however, are not only uncharged but nonpolar as well [45]. If the current proportions of amino acids reflect historic ratios, the first chirally-selected amino acids were probably nonpolar, and possibly adsorbed to a nonpolar surface.

The adsorption of proteins, polypeptides, and amino acids on solid surfaces is of interest for other reasons as well. It is now understood that biofilm formation within living systems (for example, on surgical implants such as pacemakers) and outside of them (on sanitized surfaces, where biofilms show resistance to sanitizers), usually begins with the adsorption of a layer of nonliving material, including proteins [18, 46]. This provides a point where body cells or microbes can adhere. Later, these adsorbed materials can provide a ready supply of nutrients, aiding the process of colonization. In the case of implants, adsorption of amino acids and peptides may reduce visibility to the immune system and thus improve biocompatibility. A recent study [18] suggested that the unusual ability of titanimum dioxide among the metal oxides to adsorb amino acids in solution was related to its excellent biocompatibility. Formation of external biofilms, on the other hand can be a sanitary hazard as they often confer antibiotic resistance on their resident microbes [47].

Although many of these phenomena involve proteins, the philosophy of the current

study is that isolating single-amino acid effects from phenomena associated with larger peptide behavior (such as hindered rotation about peptide bonds) may provide insight into the causes of protein behaviour. It may even be possbible to build a 'predictive' model of polypeptide behaviour at interfaces based on amino acid sequence, and recently an attempt has been made at this [25].

1.3 Equilibrium Molecular Dynamics Simulations

Molecular mechanics (MM) are a series of techniques which use sets of empirically-derived equations to model physical forces in microscopic systems. They include various energy-minimization and Monte Carlo schemes, and the very specific method of molecular dynamics (MD), which is the primary tool of investigation in the current study. In an MD experiment, Newton's equations of motion are employed to simulate physical phenomena on a scale too small to be observed directly. Because it is impossible to analytically solve the trajectory of a system of more than two interacting particles [48], the system is solved iteratively. At each step, forces between all interacting particles are determined, pair-by-pair, using molecular mechanics equations. The system is then allowed to evolve for a very short period of time before forces are again calculated.

Because only Newtonian physics is explicitly used in molecular dynamics, such a simulation cannot be used to model inherently quantum-mechanical phenomena such as bonding and chemical reactions. However, the behaviour of many systems in physical chemistry is essentially non-quantum, and the simplicity of the molecular dynamics approach allows for the simulation of systems many times the size of those which can be approached through simulation methods based on quantum mechanics. Molecular dynamics is almost unique in allowing for the explicit simulation of systems through time, although there also exist hybrid methods combining 'classic' molecular dynamics with quantum chemical methods [49, 50].

Although the equations of motion used by molecular dynamics are fundamentally

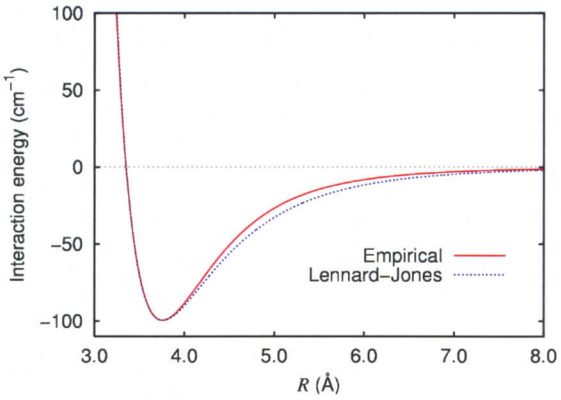

Figure 1.4: The simulated Lennard-Jones potential between two Ar atoms is very close to the experimental van der Waals potential. Force functions and parameters are chosen in molecular dynamics simulations to best reproduce experimental results. Adapted from Ref. 52, image retrieved from Ref. 53.

macroscopic in nature, the forces which they require as input often depend on quantum-mechanical properties (i.e. van der Waals forces). To bridge these disparate worlds, MD uses force fields, the sets of equations and parameters which are the basis of molecular mechanics. For example the Lennard-Jones equation is used to simulate van der Waals forces in many force fields.

$$U_{\mathrm{VdW}} = 4\varepsilon_{ij}\left[\left(\frac{\sigma}{r_{ij}}\right)^{12} - \left(\frac{\sigma}{r_{\mathrm{ij}}}\right)^{6}\right] \tag{1.1}$$

$$F_{\mathrm{VdW}} = 4\varepsilon_{ij}\left[\left(\frac{6\sigma}{r_{ij}}\right)^{7} - \left(\frac{12\sigma}{r_{\mathrm{ij}}}\right)^{13}\right] \tag{1.2}$$

In this equation r is the distance between two interacting particles, and σ and ε are parameters which depend on the identities of the particles. Both the equations and their parameters are part of a force field which is used to model the interactions of a molecular dynamics system. Force fields are typically created to reproduce a certain set of phenomena, such as free energy of solvation or freezing/melting points, and their equations and parameters are chosen to reproduce those properties (Figure 1.4. Most researchers use a force field derived by others, choosing one that was created for, or has been shown to work

well with, their system and phenomena of interest. This flexibility is both a fundamental strength and weakness of molecular dynamics. Force fields can be tailored to reproduce any desired property, but over-managing leads to facile results (the force field was tuned until the desired results were produced). Thus, discipline in choosing and staying with a force field is important in molecular dynamics studies, as is clearly explaining and sometimes justifying all the choices made in the simulation [51].

Molecular dynamics is most often used to study evolving, directional processes such as protein docking, but it can also be used to model systems in dynamic equilibrium. In these systems, bulk properties such as density are constant or almost-constant in time, and the object of study is to evaluate these equilibrium properties.

Equilibrium molecular dynamics simulations have two major requirements. First,the system under investigaion must be well-equilibrated before data collection begins. Second, the simulation must be run long enough or on a large enough scale to ensure adequate statistics are obtained to draw conclusions from. Equilibration is accomplished by evolving the system until all dynamic properties become constant with time. Typically, equilibration is preceeded by one or more energy minimizations, in which the particles of the simulation are moved toward a minimum starting potential energy. Minimizations move system toward reasonable initial forces, and purge the system of excess potential energy. This potential energy will otherwise typically become kinetic energy once the dynamics begin, leading to a spontaneous heating which can delay proper equilibration. The overall scheme for an equilibrium MD simulation is illustrated in Figure 1.5.

Equilibrium properties should be nearly constant across the system and through time. To evaluate any equilibrium property, such as the average distance between neighbouring water molecules in a simulation, it is necessary to have a breadth of measurements across time and space. In the example of water molecule distances, more measurements and a more accurate average could be obtained by increasing the number of water molecules in the simulation (leading to more measurements per timestep) or increasing the length of the

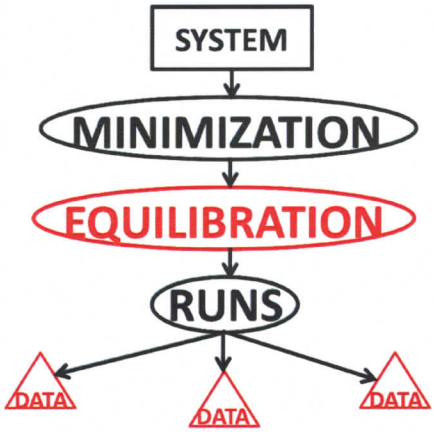

Figure 1.5: The general scheme for an equilibrium molecular dynamics simulation requires that an equilibration period precede any data collection, to ensure that the properties under investigation have stopped evolving dynamically. Most equilibrium MD simulations also require the collection of a large amount of data, since any equilibrium property will oscillate around its equilibrium value to some extent.

simulation (leading to more timesteps sampled). It is possible to increase the number of measurements without increasing their statistical relevance, however. Chiefly, this happens when timesteps very near to one another are sampled. These will carry much of the same information, and will not improve statistical sampling.

The only way to ensure better statistics are collected is to increase the size of the system or the length of the simulation. Effective equilibrium molecular dynamics simulation depends on balancing computational efficiency with the needs of the experiment [51].

Chapter 2

Methods

2.1 SPC/E and OPLS-AA/L Force Fields

Simple point charge (SPC) water was developed as a computationally-efficient model [54] which could reproduce bulk water density and heat of vapourization. Unlike more complex water models which distribute charge both over the atoms and one or more surrounding points in space, such as TIP4P [55] and TIP5P [56], SPC has charges centered only on the atoms of water, with partial positive charges of +0.41 centered on the hydrogens and a negative partial charge of -0.82 centered on the oxygen atom. All Lennard-Jones interactions are carried by the oxygen atom. Unlike most three-point water models, the bond angle of SPC water is perfectly tetrahedral (109.5°), instead of the angle suggested by experiment (104.5°).

One major weakness of SPC is that it cannot simulate the polarizability of water. SPC/E is a re-parameterization of the original SPC model [57] which attempts to account for this difference by increasing the charges on all atoms of the SPC water molecule, to $+0.4238$ for the hydrogen atoms and -0.8476 for the oxygen atom. The Lennard-Jones interaction parameters are unchanged from the SPC model. SPC/E has had success in replicating several water properties which were poorly accounted for by the original model, namely rates of diffusion in water [57].

We chose SPC/E as our model for water in this project because of its simplicity and computational efficiency, and because it was a common choice in the recent history of this

field [58, 59].

Optimized potentials for liquid simulations (OPLS) is a force field which was derived for use in simulating amino acids, peptides, and proteins [60]. It was parameterized by attempting to replicate the properties of bulk liquids which had similar functionalities as protein functional groups (i.e. ethanamine for amines-containing side-chains, and ethanol for alcohol-containing side chains).

Whereas the original OPLS was a united-atom force field, treating methyl and methylene groups as single entities, OPLS-AA/L is more recent all-atom version [61]. We chose OPLS-AA/L, with modifications (see Section 2.5, below), to simulate the intramolecular interactions within leucine and the intermolecular interactions between water and leucine for several reasons. First, the force field was derived to simulate a wide variety of peptide interactions; since the leucine zwitterion contains both charged regions and nonpolar regions, we wanted a force field versatile enough to simulate all of its components. Second, OPLS-AA/L has been shown to be compatible with the water model used in our simulations, SPC/E [60, 61].

2.2 Steele Potential and Simulation of Solid Surfaces

Solid surfaces can be simulated explicitly (with planes of bonded atoms), or with various implicit models that use functions to simulate the effect of a wall with van der Waals interactions. Explicit models have the ability to model the effects of surface structure and specific surface-solute interactions. Implicit models have the advantage of computational efficiency, and can be effective in simulating surfaces without needing to consider microscopic details like roughness. In effect, implicit wall functions allow for the examination of a wall's chemistry without the complicated or obscuring effect of its structure. In addition, because implicit walls are based on simple equations, they can be quickly and easily tuned to reflect surfaces with a wide variety of chemical properties.

For comparison with experiment, particularly vibrational sum-frequency generation

(SFG) spectroscopy, we judged a potential function to be superior to an explicit wall. An experimental surface will by necessity cover a very large area relative to the scale of a molecular dynamics simulation. For example, the smallest area which can be analysed with a sum frequency generation spectroscopy experiment is on the scale of 200 microns^2. The resulting signal will be influenced by many surface features and possibly several different planes of the surface. Only water-influencing effects which are similar at all or most surface features will be evident in the experimental spectrum. We judged these 'constant' features to be equivalent to a simple potential well - in other words, regardles of the exact structure of the surface at any given point, it will present some form of potential well to an incoming particle. The implicit function approach allows for the simulation of this 'universal' surface, which should resemble experimental results which 'average' over many individual surface features.

The surfaces used in this simulation were based on the Steele 10-4 potential, a wall model which assumes an uncharged, nonpolar surface, and integrates the Lennard-Jones potential of equation 1.1 over a two-dimensional surface.

$$U(z) = 2\pi\sigma^2\varepsilon\left[\frac{2}{5}\left(\frac{\sigma}{z}\right)^{10} - \left(\frac{\sigma}{z}\right)^{4}\right] \tag{2.1}$$

where σ describes the distance from the surface at which the potential crosses zero, and ε accounts for the depth of the well. We have fixed σ at 3 Å, and have explored values of ε ranging from 0.55–5.5 kJ·mol^{-1}. The surface-oxygen interaction potentials corresponding to our choice of ε values (Table 1) are shown in Figure 2.1, labeled according to the water contact angles described in Section 3.2.

The idea that wetting ability could be fine-tuned by altering the value of ε associated with the wall was supported by contact-angle measurements (Section 2.4). The contact angle was found to be approximately linearly dependent on ε, as can be seen in Figure 2.2. This allowed for predictable and precise tuning of surface wetting ability.

ε / kJ·mol^{-1}	z_d / Å	z_{COM} / Å	θ_c / °	θ_c surface area / Å^2
0.550	2.22	19.0	156	64×64
1.10	2.38	18.3	151	64×64
1.93	2.41	15.7	134	64×64
2.75	2.53	14.4	125	64×64
4.13	2.59	11.0	101	96×96
5.50	2.66	9.10	84	96×96

Table 2.1: Steele potential ε values for the surface-water interaction, width of depletion zone z_d, corrected droplet center of mass z_{COM}, contact angles θ_c, and surface area used for contact angle determination.

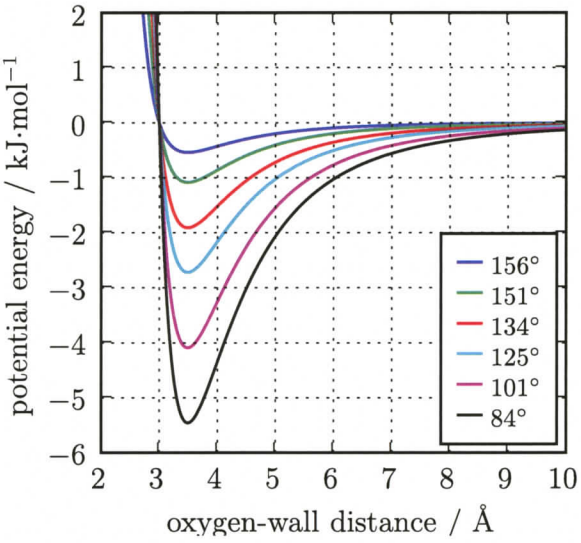

Figure 2.1: Potential energy as a function of the water oxygen-surface separation, labelled according to water contact angles.

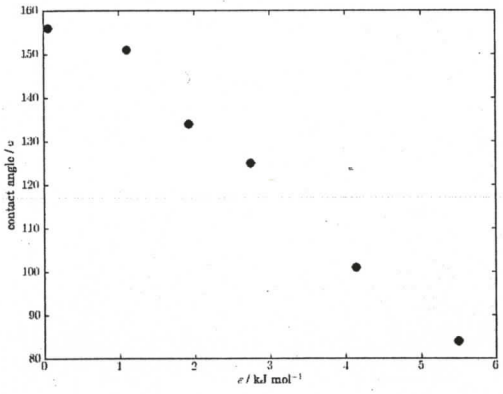

Figure 2.2: Contact angle for a given surface shows approximately linear dependence on the value of ε chosen for that surface, allowing for smooth control of surface wettability.

2.3 Simulation of Bulk Water at a Solid Interface

Simulations were performed with the GROMACS package [62], using the Verlet leap-frog integrator for equilibrations and runs. The system initially consisted of 3885 SPC/E water molecules which had undergone steepest-descent minimization and equilibration for 200 ps, in a cell of dimensions $42 \times 42 \times 70$ Å^3. Steele 10-4 potential walls were placed at $z = 0$ Å and $z = 70$ Å. Van der Waals forces were cut-off at a radius of 10 Å, while electrostatic interactions were handled with a particle-mesh Ewald (PME) summation method at long range. This method splits the electrostatic interactions of an atom into two categories. Short-range interactions are calculated using Coulomb's equation in real space; for these simulations, the short-range interactions were defined as being up to a distance of 10 Å. Long-range interactions are calculated by summing the interactions between a particle and all nieghbouring periodic cells, taking advantage of the periodic conditions of the simulation. This sum converges in reciprocal space, making it solvable. The PME method approximates atomic positions at long range as being on a repeating grid (the "mesh"), a simplification which improves computational efficiency by a large degree [51].

Each system was energy-minimized three times, using a steepest-descent method with step sizes of 0.01 Å, 0.05 Å, and 0.1 Å, respectively. The small initial step sizes helped ease the system out of starting high-energy conformations. After minimization, each system was equilibrated for 200 ps, with a step size of 1 fs. At the beginning of equilibration, velocities were randomly generated and assigned to the water molecules to achieve a net system temperature of 300 K. During equilibration and data collection, this temperature was maintained by coupling to a Berendsen thermostat [63]. Pressure was maintained at 1.01325 bar by coupling to a Berendsen bariostat [64] and allowing the box dimensions to change in the x- and y- dimensions only, since the system was isotropic over these dimensions. We have chosen a very large z dimension of 70 Å in order to have sufficient 'bulk-like' water, relatively unperturbed by the surfaces, to allow the pressure coupling to achieve a proper bulk density near 1 kg/m^3. We found that using pressure coupling with smaller boxes along the z dimension resulted in a 'bulk' density of less than 1.0 g/mL near the middle of the box, and attributed this to an inability of the pressure coupling scheme to properly account for the pressure exerted by water at the interface. As the z dimension of the simulation cell increased, the interface became proportionally less of the cell, and pressure coupling became more accurate. A 70 Å-deep box was able to reproduce a proper bulk density. Typically, pressure coupling during equilibration resulted in a change in the volume of the cell by approximately 5%.

Runs were conducted under the same conditions as equilibration, except that pressure coupling was disabled under the assumption that a well-equilibrated system will have little change in pressure over time. Figure 2.4 shows the change in box dimensions as a function of time for the 134° contact angle system, and shows that they had reached equilibrium values well before the end of equilibration. The positions of all atoms in the simulation were recorded every 50 fs. Runs proceeded for 10 ns, producing a total of 200 000 frames for analysis. Such a large data set was necessary in order to collect statistics for water species very close to the surface with sufficient resolution for systems where the density in

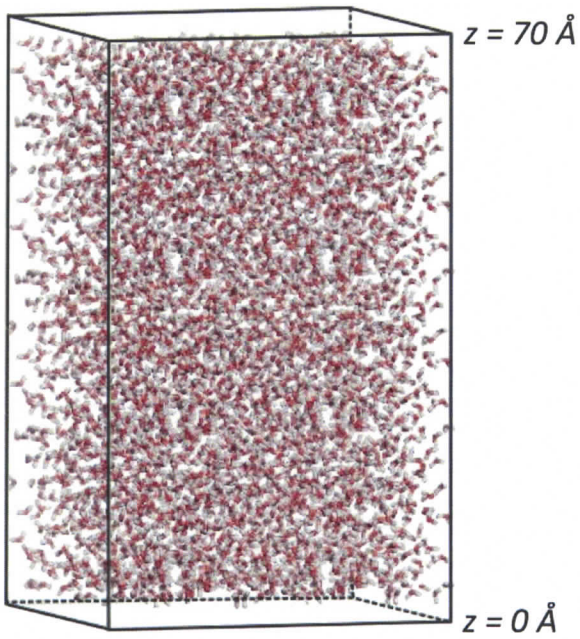

Figure 2.3: A snapshot of a bulk water system of dimensions $42 \times 42 \times 70$ Å^3 containing 3840 water molecules prior to equilibration. Steele potential walls are located at z = 0 Åand z = 70 Å.

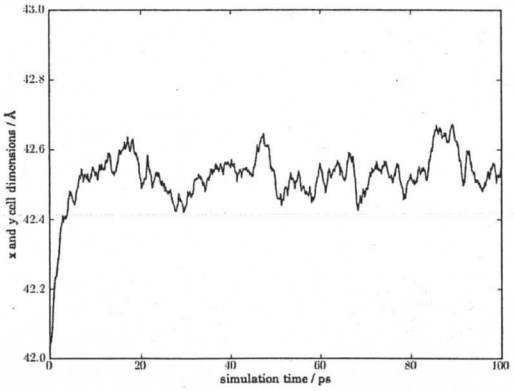

Figure 2.4: Variation of box coordinates due to pressure coupling in the $x-$ and $y-$ dimensions during the first 100 ps of equilibration. The dimensions reach equilibrium values within the first few picoseconds of equilibration.

that region was low.

Since there were two solid-liquid interfaces in each system, near $z = 0$ Å and $z = 70$ Å, a simple transformation was applied during analysis to superimpose the two interfaces. This transformation was a reflection of each atom in the simulation above $z = 35$ Åover the midpoint of the box. Due to the two-dimensional symmetry of water molecules, this rendered the two interfaces equivalent in analysis, effectively doubling our sample size.

2.4 Simulation of a Water Droplet at a Solid Interface

Simulations used to calculate the contact angles of surfaces (see Section 3.2) were similar in design to those of bulk water at an interface. The major difference was that instead of packing the system boundaries with water, a signficant gap between the water and cell borders was left in the x, y, and z dimensions. A rectangular block of 1070 water molecules covering $32 \times 32 \times 32$ Å^3, equilibrated under bulk conditions, was placed in the lower-left corner of each system. The boundaries of the system varied somewhat, but were always at least twice the dimensions of the original block of water.

Since Ewald summation methods require summation of the entire periodic cell at long range, they are more efficient in smaller boxes. Thus, we chose our box dimensions to be as small as possible. More-wetting surfaces required greater box dimensions because they encouraged the droplet to spread out during simulation, increasing the chance of one part of the droplet interacting with another across the periodic boundary conditions.

Other conditions of the previous runs, including minimization and equilibration steps, were replicated exactly since the goal was to calculate contact angles for those exact systems. The 200 ps period of equilibration was found to be adequate to allow the block of water atoms to adopt its equilibrium droplet shape.

2.5 Simulation of a Solvated Amino Acid at a Solid Surface

Where possible, the methods used to simulate pure water structure at a solid interface were repeated in simulating a solvated amino acid at the same interface. Again, simulations were performed with the GROMACS MD package. Systems consisted of 3840 SPC/E water molecules and a single zwitterionic leucine molecule, since the zwitterion predominates in solution and is most likely to be involved in adsorption under these conditions [43]. The simulation cell had initial dimensions of $42 \times 42 \times 70$ Å^3. Steele 10-4 potential walls were placed at $z = 0$ Å and $z = 70$ Å. Van der Waals forces were cut-off at a radius of 9 Å, while electrostatic interactions were handled using the PME method with a short-range cutoff of 9 Å. As in the water-surface simulations, the Steele potential walls were tuned to produce surfaces of varying wetting ability. The walls used corresponded to those in the water-surface systems, with associated contact angles of 156°, 151°, 134°, 125°, 101° and 84°.

Intra-protein interactions and protein-water interactions were handled using the OPLS-AA/L force field, with slight modifications. Harmonic terms in the potential energy function arising from dihedral positions within the protein were removed since analysis of

the conformation of leucine in the bulk and upon adsorption was of interest. Bond rotation in the amino acid was thus governed implicitly by other interactions (for example van der Waals interactions between 1 - 4 atoms). Specially-parameterized 1 - 4 interactions within the amino acid specified by the OPLS-AA/L force field were also removed, since without the accompanying dihedral parameters, their parameterization was invalid. Instead, all 1 - 4 atoms in leucine were allowed to interact as if nonbonded.

The energy of each system was minimized three times, as in the previous study. Following mimimization, to maximize computational efficiency, nine parallel simulations of each system were run simultaneously on 8 processors each. Each simulation was equilibrated separately for 200 ps with different random velocities assigned to each of its atoms at start-up. Afterwards, each simulation was run for 10 ns with data collection. Since each system contained identical components at equilibrium, and no dynamic properties were analyzed, the 10 ns runs were combined to produce the equivalent of a 90 ns trajectory of each system for analysis.

The step size in both equilibrations and runs was 1 fs. Temperature and pressure were both coupled using Berendsen methods, temperature being maintained at 300 K throughout both equilibrations and runs, and pressure being maintained at 1.01325 bar during equilibration only. As in the case of the earlier study, box dimensions changed little during equilibration, and had reached an equilibrium value after within the first 10 ps, validating the decision to remove pressure coupling during the run itself.

To render the two interfaces in the simulation equilalent during analysis, the coordinates of each atom above the midpoint of the box on the z axis were rotated 180° around the y-axis. Selection criteria were used to select only frames in which the leucine molecule was adsorbed on the surface for analysis, as is detailed in Section 4.2.

A simulation of the leucine molecule in bulk water, without any surfaces, was also conducted for the purpose of evaluating whether enough statistics were collected for our analysis. The orientation of leucine in bulk water appears in Figure 4.4 as a 'baseline' to

compare to the results of the other systems. The bulk water simulations were conducted exactly as the surface simulations described above, except the system had only 2477 water molecules in a cell of dimensions $42 \times 42 \times 42$ Å^3.

Chapter 3

Interfacial water structure at surfaces of varying wettability

3.1 Background

In recent years, it has become clear that the physical and chemical properties of heterogenous systems are often dependent on water molecules at the solid interface [6, 65].

Theoretical solid interface studies to date have examined the interaction between water and structured polar [66–72] and nonpolar [58, 72, 73] surfaces. There have been relatively few studies of water interacting with isotropic surfaces, yet such studies permit investigation of water structure as a function of only the surface-water potential energy, and can therefore be generalized to many surfaces.

Simulations to date have agreed on a few features of the water-solid interface. 'Hard' surfaces, those in which repulsive potential rises abruptly, lead to oscillations in density which can extend well into the bulk even in the absence of any attraction between water and surface, although any such attraction will tend to increase the magnitude of the oscillations [74]. In contrast, 'soft' surfaces, in which repulsive potential rises more slowly such as at liquid-vapor or liquid-liquid interfaces, will have a sigmoidal increase in density as one moves from the interface into the bulk [75].

The orientation of water molecules at a solid-liquid interface was first elucidated by Lee and Rossky in 1984 [72] Their simulations indicated that water molecules immediately

adjacent to the surface tend to project one hydrogen-bonding group toward that surface. By sacrificing this bond, the molecules are able to preserve three other hydrogen-bonding groups by pointing them into the bulk; the result is that interfacial molecules have on average approximately three hydrogen bonds, instead of just two that would be predicted if they maintained bulk structure at the interface. Most theoretical work has echoed these results [73,76].

Our own experiments confirmed the density-related findings of previous experiments, but revealed another type of water ordering which had only been partially described once before [58], in a study of a somewhat more-wetting surface than Lee and Rossky's, In this structure, water molecules at the interface were tilted such that their symmetry axes were nearly perpendicular to the surface. This structuring was rarely observed because previous experiments with nonpolar surfaces only described very non-wetting interfaces; when wetting surfaces were simulated, they were polar and structured. Although it is true that most natural wetting surfaces are polar, the hydrophobic surfaces utilized in studies such as Lee and Rossky's were extremely non-wetting, possessing a contact angle of more than 150° by our calculation. There are many nonpolar surfaces which are more-wetting than this; we refer to these as 'semi-wetting' surfaces.

Our current study provides an explanation for both sets of observations in the literature, based on the existence of two water structure regimes, non-wetting and semi-wetting. We propose that the crossover between these regimes occurs when a surface has a contact angle around 130°. We also examine the implications of the existence of the semi-wetting regime to experimental studies, particularly SFG experiments indicating the lack of a coupled hydrogen bond at wetting surfaces.

3.2 Contact Angles

In order to determine the wetting characteristics of surfaces parameterized by a particular set of Lennard-Jones σ and ε parameters, we have determined their water contact angles,

θ_c. There have been several schemes proposed for this in the literature [77–79]. A simple method that has been shown [79] to produce results nearly identical to more sophisticated schemes is to determine the corrected mean center of mass $\langle z_{\mathrm{COM}} \rangle$ of a droplet on the surface, and then relate this to the radius of a free droplet R_0 via

$$\frac{\langle z_{\mathrm{COM}} \rangle}{R_0} = \frac{2^{-4/3}(3+\theta_c)}{2+\theta_c} \left(\frac{1-\theta_c}{2+\theta_c} \right)^{1/3}. \tag{3.1}$$

R_0 was calculated from a simulation of a free droplet consisting of 1070 SPC/E waters. The radius of this sphere was determined by calculating the distance from the center of mass to the furthest oxygen atom in each of three orthogonal directions, averaged over multiple frames of the trajectory. z_{COM} for each surface was calculated from simulations of the same 1070 water molecules when placed in a rectangular cell of sufficiently large surface area with Steele potential walls at z = 0 Åand z = 70 Å. We analyzed frames of a subsequent 1-ns trajectory in order to determine the distance between the mean center of mass along z and the oxygen atom closest to the surface. This was then used as $\langle z_{\mathrm{COM}} \rangle$ in Equation 3.1. Edge-on views (looking down x) of arbitrary frames are shown in Figure 3.1 for illustrative purposes.

Contact angles thereby determined for all systems are listed in Table 1. The system with the most shallow surface-oxygen potential, corresponding to $\varepsilon = 0.55$ kJ/mol was determined to have $\theta_c = 156°$; the most attractive surface with $\varepsilon = 5.5$ kJ/mol displayed $\theta_c = 84°$. From here on, each of these systems will be referred to by its respective water contact angle (CA).

3.3 Density Profiles

Density profiles for each of the systems studied are shown in Figure 3.2, binned with a resolution of 0.01 Å, and labeled according to their water contact angles. Very non-wetting (151,156° CA) surfaces had the simplest behavior, with only small variation in the density from the bulk approaching the interface. At around 5 Å from the surface, the density

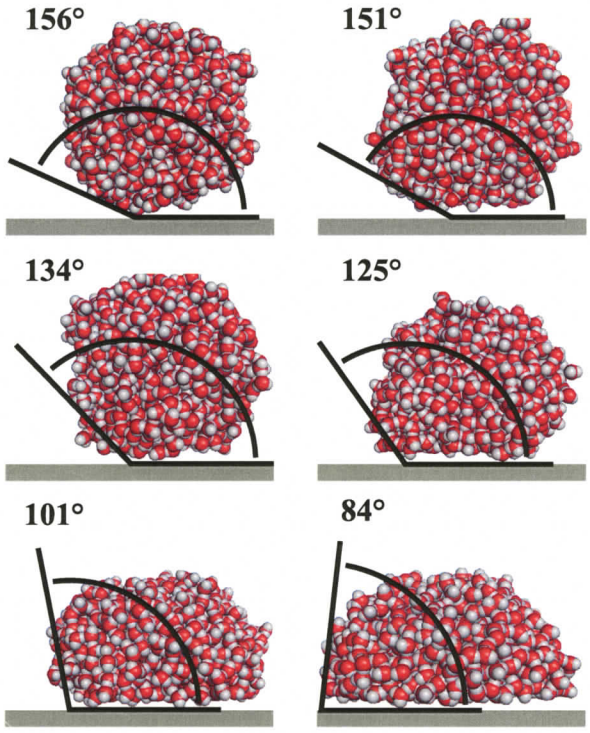

Figure 3.1: Water contact angles for the six surfaces we have studied. These figures are snapshots of the 1070 water molecules used for this determination. Tangent lines and drawn angles are for illustrative purposes only. The actual contact angles were determined from statistical analysis of many frames in the trajectory, as described in the text.

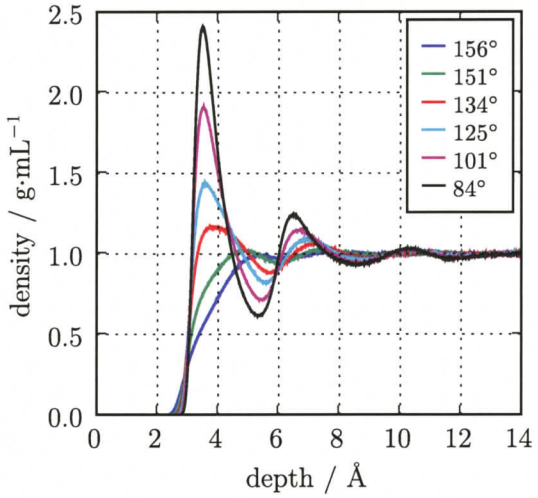

Figure 3.2: Density profiles as a function of the distance from the surface. Two patterns of structure are apparent. At the least-wetting surfaces, there is a sinusoidal increase from zero density to the bulk level across the interface. At the most-wetting surfaces, there is an initial region of high water density followed by alternating regions of low and high density.

gradually drops towards zero. The more-wetting surfaces display a more complex behavior, with oscillations in the density still visible ≈ 13 Å into the bulk water phase. As a result of van der Waals repulsion, sharp peaks in the density are paired with adjacent regions of low density. All surfaces with contact angles less than 150° display a sharp peak near 3.5 Å, a dip near 5.5 Å, and a second peak around 6.5 Å. It is evident that the location of these latter two features occurs closer to the interface as the surface becomes more wetting.

Overall, density profiles were found to change in a smooth, predictable fashion as the contact angle of the surface changed. Examination of these trends resulted in two types of surface being identified. Non-wetting surfaces showed a smooth, sigmoidal decay in density, mimicking the behaviour of the air-water interface which has previously been well-studied [6, 80–83]. More-wetting surfaces had a region very close to the surface in which water density was greater than in the bulk, and showed oscillating density well into the bulk. The transition between these two regimes appeared gradually around a surface contact angle of 130°.

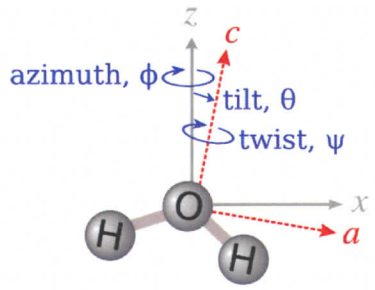

Figure 3.3: This figure illustrates the convention that we use to describe the cartesian coordinates (a, b, c) in the molecular frame and (x, y, z) in the lab frame. For simplicity, this is illustrated with the molecular b-axis aligned with the lab y-axis, both directed into the page. The water molecule is in the ac-plane with c parallel to its C_2 rotation axis. The tilt angle θ is the angle between the surface normal z and the molecular c-axis. The twist angle ψ describes rotation about the molecular c-axis.

3.4 Orientation Analysis

In order to describe the structure of water adjacent to these surfaces, we parameterize the orientation in terms of three Euler angles. As illustrated in Figure 3.3 we define the molecular coordinates so the molecule lies in the ac plane; θ is the polar angle between the water symmetry axis (molecular c axis) and the surface normal, z; ϕ is the azimuthal angle about the surface normal; ψ is the twist angle about the molecular c axis.

In each system, we have determined these Euler angles for every water molecule, and then binned the results with 1 Å resolution. Tilt and twist histograms as a function of distance from the surface are shown in Figure 3.5 for surfaces with contact angles of (a,b) 156°, (c,d) 151°, (e,f) 134°, (g,h) 125°, (i,j) 101°, and (k,l) 84°. Each histogram is scaled independently so the highest population appears dark red and lowest population is dark blue. We have not displayed azimuthal (ϕ) histograms, as we have determined the azimuthal distribution to be completely uniform. This is expected since our surfaces are isotropic, with no ability to order molecules in the xy plane. For the non-wetting surfaces, molecules closest to the interface, located at $z = 2.5$ Å, exhibit a fairly narrow tilt distribution centered at $\theta \approx 70°$ (Figure 3.5a) and twisted such that $\psi = 0°$ (Figure 3.5b.

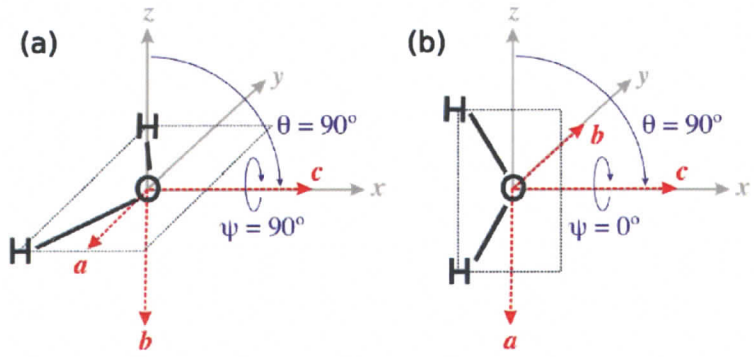

Figure 3.4: Two orientations of a water molecule illustrated with accompanying Euler angles θ and ψ. When θ and ψ are each equal to 90°, the water molecule lies in the plane of the interface; when θ is 90° and ψ is 0°, the water molecule lies perpendicular to the surface, 'straddling' the interface.

The histogram reveals that $\psi = 180°$ is equally populated; this is an equivalent orientation to $\psi = 0°$ due to the C_{2v} symmetry of the water molecule; we display $0° < \psi < 180°$ for clarity.) This indicates that these water molecules direct one of their hydrogens towards the surface. The next layer of waters, located at $z = 5$ Å, has a more diffuse tilt distribution centered at $\theta = 90°$, and a well-defined twist distribution centered at $\psi = 90°$. These waters are lying in the plane of the interface. As the wettability of the surfaces increases, the tilt distribution of adjacent water molecules gradually shifts from 70–90°, and their mean twist angle rapidly moves from 0° to 90°. We therefore find that surfaces with a greater tendency for wetting have in-plane water molecules in close proximity. The adjacent layer of water molecules ($z \approx 5$ Å) displays a different trend. Their tilt angles increase from $\approx 90°$ in the case of the non-wetting surface (a) to $\approx 130°$ for the most-wetting surface (k). Their twist angle distributions remain centered at $\psi = 90°$ as they move away from the non-wetting surfaces (b,d), but become narrower. Looking at the surface with contact angle 134° (f), we see that the twist distribution of these second layer of waters is broader than those immediately adjacent to the surface; by the time we approach a contact angle of 84° (l) the twist distributions of both water layers are equally narrow. Our final observation is that the

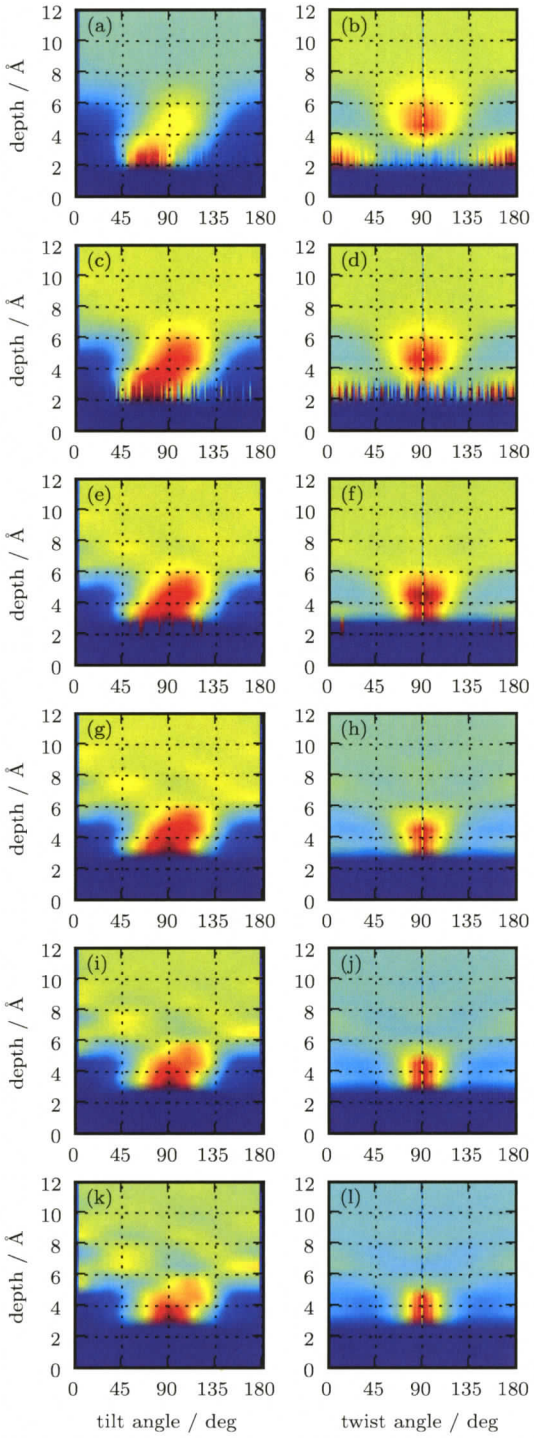

Figure 3.5: Angular histograms showing the tilt and twist angle distribution as a function of distance from the surface. Plots a–l are identified in the text.

tilt angle distribution becomes more complex and extends further into the bulk water phase as the surface wettability increases. This is seen as a smooth progression in all the systems studied, but is exemplified in (k), where distinct ordering is observed up to $\approx$ 10 Å from the surface.

Although these angular histograms provide direct information about the water orientation, they do not lend themselves to facile comparison between the systems. One reason is that they cannot be easily interpreted if they are overlaid. Furthermore, since features in the histograms are apparent only if each histogram is scaled accordingly to its maximum value, it is difficult to quantitively determine how ordered the various systems are. We address these issues by computing order parameters for the tilt and twist angles, and binning them according to their distance from the surface with 0.2 Å resolution. The average tilt order in each 0.2 Å bin is defined by

$$S_\theta = \frac{1}{2}\langle 3\cos^2\theta - 1\rangle \tag{3.2}$$

where the angular brackets denote an ensemble average over all tilt angles. A value of $S_\theta = 1$ indicates that water molecules are perfectly aligned with their symmetry axes along the surface normal. If all molecular c axes are instead perpendicular to z, we would observe $S_\theta = -0.5$. An isotropic tilt distribution would have $S_\theta = 0$. Tilt order parameters for all systems are shown in Figure 3.6a. We see that past $\approx$ 14 Å we have $S_\theta = 0$, indicative of isotropic bulk water. Closer to the interface $S_\theta \neq 0$ indicates interfacial ordering with respect to the water symmetry axis. The simplest behavior is displayed by the non-wetting systems. Moving from the bulk towards the surface, their tilt order parameters monotonically take on larger negative values. Closest to the surface, $S_\theta = -0.24$ indicates strong ordering with $c \perp z$. The depletion region is shaded light gray in the figure. The narrow dark region does contain water molecules, but insufficient numbers to have meaningful statistics for computing order parameters, so there is a small region in which we have no information. We have used very long trajectories (200 000 frames over 10 ns) in order to minimize the width of this non-reporting region. As the

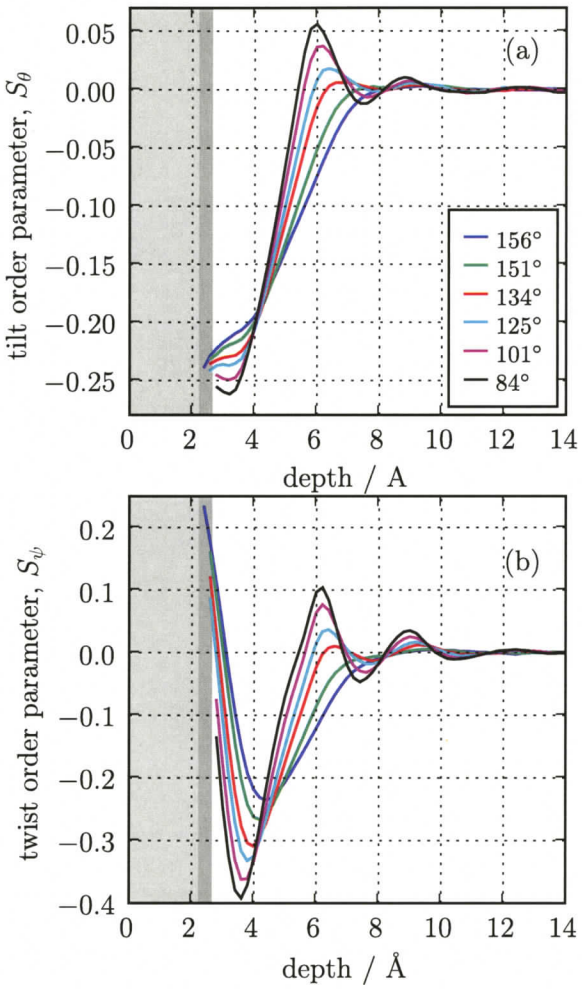

Figure 3.6: Order parameters as a function of the distance from the surface. (a) Tilt order parameter, describing the alignment of the water symmetry axes with respect to the surface normal. (b) Twist order parameter, describing rotation about the water symmetry axis. The light gray area indicates the depletion region immediately next to the surface where no water molecules are found. The darker shaded strip indicates a region of non-zero water density, but poor statistics for order parameters as a result of the very low density.

surfaces become more-wetting, the tilt order parameter takes on significant positive values at $z = 6$ Å, indicating that the preferred alignment is closer to $c \parallel z$. At $z \approx 5$ Å the order parameter switches sign and becomes increasingly negative closer to the surface. For the most-wetting systems, relatively far from the surface we observe the tilt order oscillating about zero. This corresponds to the layered structure we observed in the tilt histograms. An interesting subtle feature not evident in the histograms is that the least-wetting systems become increasingly ordered close to the surface, yet the most-wetting systems have less order at $z \approx 3$ Å. In general, however, the extent of the ordering increases with surface wetting ability.

The twist order is obtained from

$$S_\psi = \frac{\langle \sin^2\theta \cos 2\psi \rangle}{\langle \sin^2\theta \rangle}. \tag{3.3}$$

Here a value of $S_\psi = 1$ corresponds to $\psi^* = 0/180°$ for all molecules, while $S_\psi = -1$ corresponds to perfect alignment with $\psi = 90/270°$. A value of zero indicates a uniform twist distribution. Twist order parameters for all systems are shown in Figure 3.6b. Again, the non-wetting systems have the simplest behavior. At distances greater than $z \approx 9$ Å, $S_\psi = 0$ indicates isotropic bulk water. In the region 3 Å $< z <$ 9 Å, the twist order is negative, indicating that molecules prefer to align with ψ closer to 90°. Very close to the surface, this parameter is now positive, indicating that ψ is now ordered more towards 0°. As the wetting ability of the surface increases, we observed oscillations in the twist order at some distance from the surface, followed by positive values at $z \approx 6$ Å, and then negative values for regions $z < 5$ Å. Immediately next to the surface, we see that the most-wetting system maintains a negative twist order, whereas less-wetting systems have twist orders that become positive in this narrow region. There is a tendency for the molecules at both wetting and non-wetting surfaces to favor lying with their dipoles parallel or nearly parallel to the surface, which is more pronouced in the semi-wetting surfaces. The two regimes differ in the sign of their twist angle near the surface, implying that the molecules of one regime are perpendicular to the other. The semi-wetting surfaces also appear to have a

more pronounced ordering near the surface and further away (greater deviation of both tilt and twist order parameters from zero).

3.5 Hydrogen Bonding Analysis

We can obtain further insight into the characteristics of the interfacial environments by studying the nature of the hydrogen bonding between water molecules. Previous studies have assessed hydrogen bonding according to distance [84], distance-angle [85, 86], and energy [87, 88] criteria. It has recently been concluded that a simple intermolecular H—O cutoff provides excellent performance, and sacrifices little compared to more computationally-expensive H-bonding criteria [89]. We define two water molecules as being hydrogen-bonded if their intermolecular H—O distance is less than 2.5 Å. On this basis, we determine the average number of hydrogen bonds as a function of distance from the surface, binning with a width of 0.2 Å. Figure 3.7a indicates the fraction of water monomers (those molecules not making any hydrogen bonds) as one moves from the surface towards the bulk. This species becomes more populated as the surface becomes less-wetting, but the total population hardly exceeds 0.1% of all H-bonding coordination states. At distances greater than 6 Å from the surface, there are virtually no water monomers. Figures 3.7b,c,d display the fraction of water molecules making one, two, and three hydrogen bonds, respectively. In the bulk, they correspondingly comprise $\approx$ 0.2%, $\approx$ 4%, and $\approx$ 27% of the population; they are enhanced in the interfacial region. (b) One- and (c) two-coordinated species behave as the monomers, with increased population next to less-wetting surfaces. The behavior of the three-coordinated species (d) is a bit more complex, showing some oscillations in the population in the regions of 7 and 9 Å. Up until 4 Å from the surface, less-wetting surfaces show an increasing enhancement for three-fold H-bonding coordination relative to the bulk. Closer than 4 Å, the trend reverses. The 3-fold coordination peaks and then drops, with the non-wetting surfaces peaking earlier, at a lower population, and more quickly than the surfaces with a greater wetting tendency.

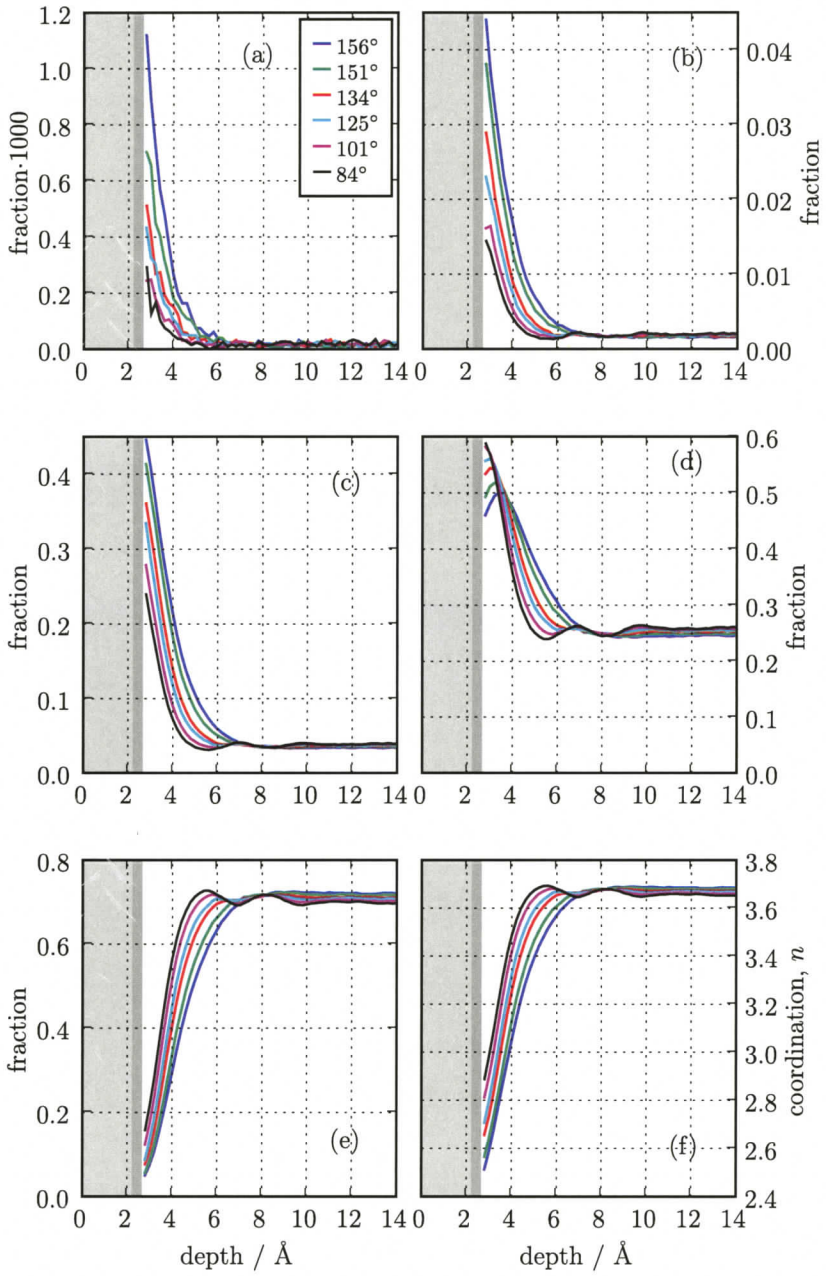

Figure 3.7: Number of hydrogen bonds as a function of the distance from the surface. (a) Monomers, water molecules that are not making any hydrogen bonds; (b) single-coordinated species; (c) 2-coordination; (d) 3-coordination; (e) tetrahedrally-coordinated species; (f) average number of hydrogen bonds. The light gray area indicates the depletion region immediately next to the surface where no water molecules are found. The darker shaded strip indicates a region of non-zero water density, but poor statistics for hydrogen-bonding analysis as a result of the very low density.

Closer than 2.6 Å it becomes difficult to comment on these trends since the population of interfacial water species is low. Still, obvious trends have been established before this point. Figure 3.7e shows tetrahedrally-coordinated water molecules. In the bulk, these comprise just over 70% of all water molecules. In the interfacial region, their fraction drops to 10–20%, with less-wetting surfaces exhibiting the smallest fraction of four-coordinated species. These details are summarized by displaying the average number of hydrogen bonds, n, as a function of distance from the surface in Figure 3.7f. For the least-wetting systems, we see that this value decreases in the interfacial region, dropping below $n = 2.6$ closer than 3 Å from the surface. For surfaces with greater tendency for wetting (contact angle as low as 84°), it is interesting to observe that there is a region of the interface (near 5 Å) that displays a greater number of hydrogen bonds than bulk water. On closer approach, the average coordination drops. In general, less-wetting surfaces are less coordinated in the interfacial region. The semi-wetting surfaces show a greater ability to retain hydrogen bonds close to the interface, as well as a region of improved hydrogen bonding adjacent to the interface. For the 84° CA surface the average number of hydrogen bonds per molecule increases to $n \approx 3.7$ from a bulk level of $n = 3.66$.

Chapter 4

Amino acid absorption on surfaces of varying wettability

4.1 Background

As was discussed in Section 1.2, protein adsorption on solid surfaces is a phenomenon of broad interest. Protein adsorption at a hydrophobic surface is complex, and depends on a variety of interactions between surface, solvent, and protein, and within the protein [90,91]. In general, however, proteins have a greater affinity for adsorption than single amino acids do, and show coniderable resistance to being displaced by other proteins [38].

Although molecular dynamics simulations of whole proteins and surfaces exist [92] they remain too computationally expensive to apply systematically to predict protein adsorption with a high degree of accuracy. Schemes for evaluating the hydrophobicity or hydrophilicity of proteins and protein regions based on amino acid sequence have been used for some time [24] to evaluate the behaviour of proteins in cell membranes. Similar schemes have recently been proposed for evaluating protein adsorption on solid surfaces [25], but these are complicated by needing to consider the varying effects of solvent and surface. The improvement of these methods will require better knowledge of how different amino acids interact with different surfaces.

There is still considerable debate about amino acid adorption at solid surfaces, in large part because adsorption can be driven by different factors depending on the amino acid and

surface examined. More work has been directed to examining the adsorption of amino acids on polar surfaces than hydrophobic ones, both in experimental [31, 32, 39, 40, 93, 94] and computational work [95–98]. The majority of theoretical studies to date have excluded the possibility of significant hydrophobic interactions between surface and amino acid entirely, by using glycine as their model for adsorption [43].

When adsorption of amino acids to polar or charged surfaces is observed, experimentally, it tends to involve chemical reactions such as hydroxyl transfers which are often not reversible [95, 99] and in which desorption can involve fracturing of the molecule [18, 96]. The other major mode of adsorption for these surfaces is ion - ion interactions between acidic or basic amino acids at a pH where they carry a net charge and charged surface sites such as danging oxygen atoms at SiO_2 surfaces [33,45,93]. The former mode of adsorption is unacceptable for applications such as chromatography, which depend on reversible and rapid adsorption and desorption, and is also not relevant to study of processes like chiral selectivity, which require an adsorption process which retains the whole amino acid. The latter mode is useful to separate charged amino acids, but not applicable to others. In addition, because the reactivity of these surfaces depends on specific interactions between surface sites and amino acid groups, their behaviour is often highly dependent on variables. These variables include the density of relevant groups at the surface [35] and the extent of surface hydroxylation [95], as well as conditions in the aqueous phase such as pH [40, 99]. The ability to modify these factors may be useful for tuning properties of adsorption, but the need to control them creates an obstacle for industrial applications.

Reversible adsorption of amino acids is thus a topic of considerable importance. The consensus of literature [30, 32, 93, 100] is that adsorption is largely a hydrophobic effect, driven for most amino acids by the interaction of their side-chains with a surface and the water near that surface. The role of water as solvent is crucial in reversible adsorption of amino acids; While polar and hydrophilic surfaces can reversibly adsorb all amino acids *in vacuo* [96], they tend to have great difficulty adsorbing them in aqueous environments [18,

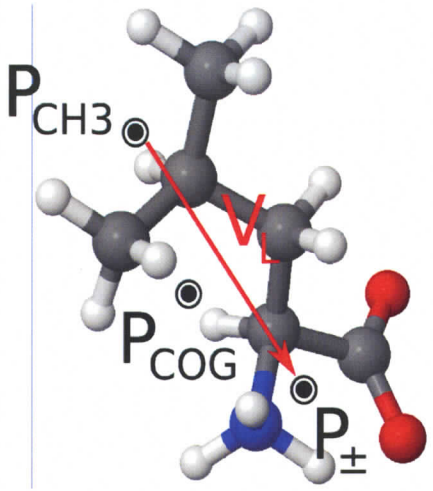

Figure 4.1: The leucine molecule, with the positions of the center of geometry, center of charge, and average methyl position labelled as well as the long axis vector.

34,95]. This implies that the role of water is crucial in promoting or preventing adsorption, and by extension in determining adsorbed structure.

Our simulations are well-placed to provide a complementary view to the body of literature regarding amino acid adsorption on charged or polar surfaces. Our surface is neither structured nor charged. The effects of adsorption are thus reduced to cooperation between water and leucine through solvation, and competition between water and leucine for adsorption to the surface. Our studies focuses are the interaction of an adsorbed amino acid with a nonpolar surface, and the role water plays in that interaction.

4.2 Trajectory Sampling

All analyses were conducted using several reference points and vectors illustrated in Figure 4.1. The molecule's center of geometry, P_{COG}, was located by averaging the location of every atom in the molecule. The center of geometry was chosen as a reference point for analysis because it provided a measurement of leucine's position which was independent of leucine's conformation.

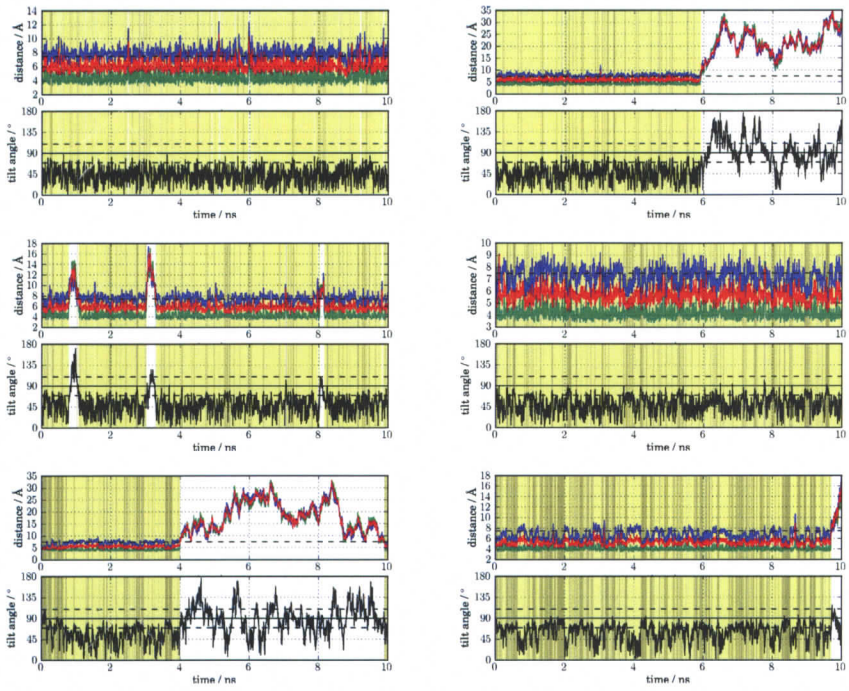

Figure 4.2: Sampled properties for each system over a 10 ns trajectory. The upper plot shows the positions along the z-axis of the center of charge (blue), center of geometry (red), and average methyl position (green) of leucine. The lower plots show the angle of the long axis vector relative to the surface normal.

Two other points were defined for analysis. $P_{\pm}$ was defined as the average of the position of the amine nitrogen and carboxyl carbon. It was intended to provide a measurement of the location of the most hydrophilic, charged portion of the leucine molecule. P_{CH3} was defined as the average of the positions of the two carbons of the methyl groups that terminate leucine's side chain. It was chosen to provide a measurement of where the most-hydrophobic, nonpolar regions of the leucine molecule were located.

The vector running from P_{CH3} to $P_{\pm}$, V_L, was chosen to measure leucine's orientation with respect to the surface. This vector runs along the longest axis of the molecule regardless of its conformation.

The initial analyses conducted involved sampling the positions of P_{COG}, $P_{\pm}$, and P_{CH3}.

Since the systems were isotropic in the x and y dimensions, position was recorded along the z axis only, and the angle of the long axis vector was calculated relative to the surface normal. Figure 4.2 shows one 10 ns trajectory for each of the systems studied; each trajectory was chosen randomly from the nine simulations completed in parallel. The trajectories were sampled every 100 frames, or 5 picoseconds.

This analysis provided a picture of how the systems evolved dynamically, and what behaviours were associated with one another. From Figure 4.2, the timescales of events such as shifts in orientation and leucine's adsorption and desorption from the surface can be estimated, and were found to occur well within the period of the simulation.

The trajectory analyses confirmed for us that leucine was leaving the surface for some period of time in each simulation and was tumbling freely during this time. This was important because it indicated that leucine was able to sample the full range of orientations it had access to in the bulk, and was not excessively prejudiced toward the orientation it assumed upon initial adsorption.

Based on the results of Figure 4.2, P_{COG} was chosen as the criterion for whether leucine was considered adsorbed to the surface or not in other analyses. If the molecule's center of geometry had a z-coordinate less than 7.5 Å, it was considered adsorbed to the surface (indicated in Figure 4.2 by the yellow shaded regions).

White regions show where the leucine molecule left the surface; the fact that leucine was capable of desorption and re-adsorption within the simulation was a positive sign, as both occur in real systems [32, 34, 35]. Desorption also allowed leucine to approach the surface again with different orientations, as is evidenced by the large variation in long axis angle when the molecule leaves the surface.

The positions of $P_{\pm}$ and P_{CH3} relative to one another were consistent when adsorbed throughout every trajectory. Leucine always adsorbed with $P_{\pm}$ above P_{CH3}. Usually, the difference in z position between the points was about 4 Å, but there were periods, mostly in trajectories of the most-wetting systems (84° and 101° CA), in which the position of the

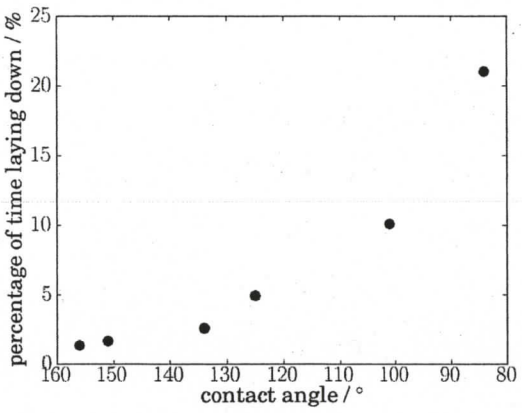

Figure 4.3: The fraction of snapshots along each trajectory in which leucine is adsorbed in the laying orientation increases in what appears to be a sigmoidal fashion as wetting ability of the surface increases.

center of charge would move toward the surface by between 1.5 and 2.0 Å, and the average methyl position would move in the same direction approximately 0.5 Å, with the result that the molecule appeared to be flattened out. These periods became more-frequent and longer-lasting in the more-wetting systems, as is shown in Figure 4.3.

Accompanying this change in atomic positions was usually a change in orientation, signalled by a change in the angle between V_L and the surface normal. For most of each simulation, this angle remained less than 60° when the molecule was adsorbed, but when $P_\pm$ approached the surface the angle typically jumped to above 70°, supporting a conclusion that during these periods leucine was temporarily lying flat against the surface. The laying periods were defined as those in which the angle between V_L and the surface normal is between 70–110°, which are the dashed lines in the angular plots of Figure 4.2. The periods in which leucine was considered by this criterion to be laying on the surface are highlighted in Figure 4.2 in grey.

Torsional angles were originally part of this analysis, but the timescale of torsional angle rotation (in particular, the difficulty in sampling the least-stable conformations) was

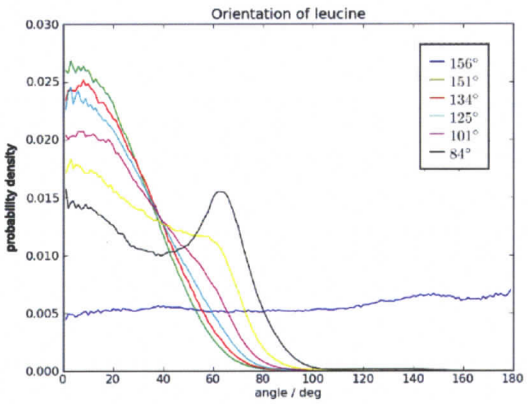

Figure 4.4: Histogram showing orientation angles adopted by leucine's long axis vector with respect to the surface normal over 90 ns of analysis.

found to be too large for this simulation. The qualitative indications of this analysis were that adsorbed conformations did not significantly differ from those in the bulk, supporting a decision to study only the orientation of adsorbed leucine.

4.3 Orientation Histogram

A histogram was constructed to more quantitatively examine leucine's orientation at the surface. Every 50 frames of the simulation, if P_{COG} was < 7.5 Å, a snapshot was taken for analysis. The angle of V_L with respect to the surface normal was binned for each snapshot to 1° resolution. Each bin was divided by the sine of its associated angle to normalize with respect to an isotropic orientation distribution.

The results of a bulk trajectory analysis were also included in Figure 4.4. Ideally, the results of the bulk analysis should have shown equal counts for all angles between 0° and 180°. The deviations below 40° and above 140° must unfortunately be regarded as due to insufficient statistics.

When combined with the results of the trajectory analysis, Figure 4.4 suggests the existence of at least two distinct orientational states for leucine on the surfaces studied.

In particular, the distinctness of the peak at 50° in the histogram for the 84° CA surface implies that rather than exhibiting variation in orientation angle around a single preferred orientation, leucine favored two orientations and switched between then while adsorbed.

4.4 Atomic Density Profiles

To determine the orientation of adsorbed leucine more precisely and compare the properties of the two orientation states, density profiles were constructed for P_{COG}, $P_{\pm}$, and P_{CH3}. Separate profiles were created for the standing and laying orientations of leucine, which were distinguished using the angular criterion discussed earlier. Each plot in Figure 4.5 shows the standing and laying density profiles associated with one surface, together with the density profile of pure water for the same system. Standing orientations are distinguished with solid lines, and laying orientations with dashed lines. As in Figure 4.2, P_{COG} is red, $P_{\pm}$ is blue, and P_{CH3} is green. The density profile of pure water at the same surface is the solid black line. All density profiles have been normalized so that the y-axis corresponds to probability density, and the area under each curve sums to unity.

Several results from these analyses are apparent. Across all systems and both orientations, P_{CH3} is closer to the surface than P_{COG}, and $P_{\pm}$ is further from the surface than P_{COG}. In the standing orientation, the separation between P_{CH3} and $P_{\pm}$ is greater than in the laying orientation. In the laying orientation, $P_{\pm}$ moves considerably closer to the surface, while P_{CH3} moves somewhat further away from it. As surfaces become more-wetting, the movement of $P_{\pm}$ becomes more pronounced, and the movement of P_{CH3} becomes less so.

For the least-wetting surfaces, there is greater freedom of movement for P_{CH3}, $P_{\pm}$, and P_{COG} when in the laying orientation. For the most-wetting surfaces, the reverse is true for P_{COG} and $P_{\pm}$ but P_{CH3} remains most tightly distributed in the standing orientation. Although P_{CH3} in the most-wetting surfaces is very tightly distributed, there begin to emerge two peaks for each of P_{COG} and $P_{\pm}$ when in the standing orientation.

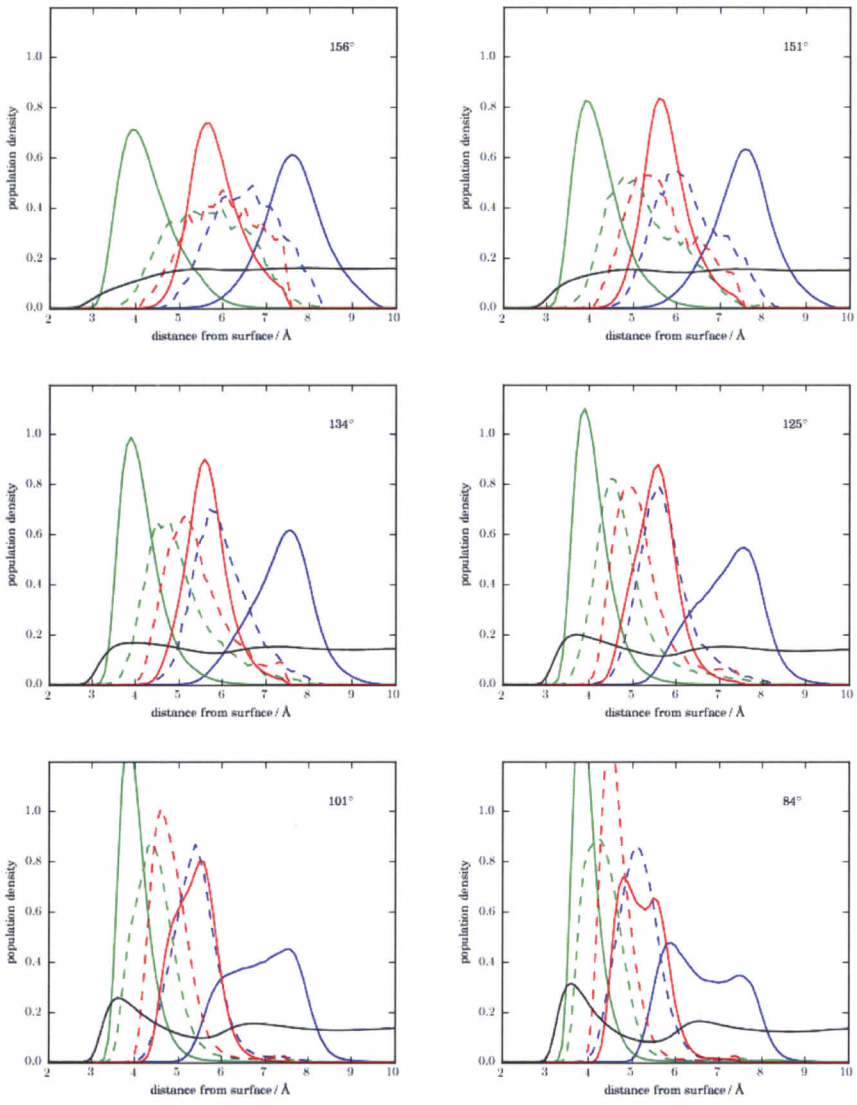

Figure 4.5: Density profiles for the position of leucine's center of geometry (red), center of charge (blue), and average methyl position (green) when adsorbed on the surface. Solid lines depict positions when leucine is in the standing orientation, dotted lines show positions when the molecule is in the laying orientation. The solid black line shows the probability density of water molecules in a water-only simulation at an equivalent surface.

Chapter 5

Discussion

A new regime of water ordering was seen at simulated surfaces of contact angle less than 130°. The explanation for the existence of this regime, and why it departed from structures seen at less-wetting surfaces, relied on an analysis of the density structure of water at solid surfaces. This density-dependent model of structuring was then applied to analysis of leucine's adsorption at the same hydrophobic interfaces with some success, suggesting that density analysis may be a generally-effective tool for studying adsorption and interfacial structure.

5.1 Model of density-dependent alignment of water

Three kinds of analyses were conducted: density profiles, orientation analysis (including angular distributions and order parameters), and hydrogen-bonding profiles. In each of these, we observed a smooth transition from a non-wetting to a semi-wetting regime. This implies that these factors are interconnected in determining the nature of interfacial ordering. Semi-wetting surfaces favor surface-water interactions, which leads to a high density of water close to the surface. Non-wetting surfaces favor water-water interactions, which results in structures that promote a maximum number of hydrogen bonds at the surface. We now propose a model that accounts for the structure of water next to solid surfaces of varying hydrophobicity. Afterwards, we will discuss our results and this model together with experimental observations in the recent literature.

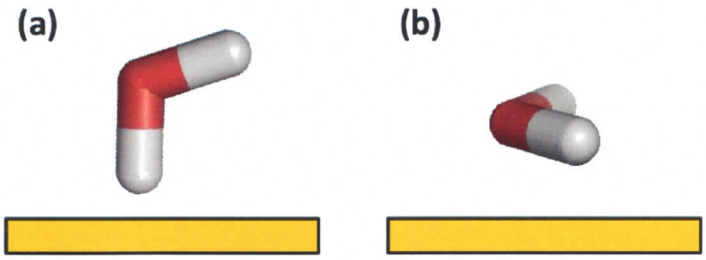

Figure 5.1: Water molecules closest to the surface adopt different orientations at non-wetting and semi-wetting interfaces. In the non-wetting ordering regime (a), interfacial water molecules orient themselves to point one O-H bond toward the surface, while in the semi-wetting regime (b) they come to lie in the plane of the surface.

Across the hydrophobic surfaces considered, a transition between two realms of water ordering is observed, defined by the orientation of the water molecules closest to the surface as shown in Figure 5.1. In the least-wetting systems water molecules nearest the surface orient themselves to point one hydrogen atom towards the interface, allowing them to project three hydrogen bonding groups towards the bulk. The non-wetting structures are thus analogous to the structure of the well-characterized [81, 83] air-water interface. Lee and Rossky explain that by adopting the observed geometry, interfacial water molecules preserve a net hydrogen bond they would otherwise lose. They have specifically shown that introducing a hypothetical surface into bulk water without allowing the molecules to re-orient themselves results in interfacial water molecules having an average of only two hydrogen bonds [72]. We have implemented the description of the hydrophobic surface from Ref. [72], together with SPC/E water and have determined the contact angle to be approximately 150°. This places their surface well within the non-wetting regime, and therefore lends support to our observations. As the wetting ability decreases, however, we observe a transition to a new interfacial structure. In the semi-wetting structures, water molecules orient themselves to lie in the plane of the surface. This coincides with an increase in water density close to the surface. This is similar to the structure of water observed at an ice-like surface that was set up without surface polarity [58].

We propose the following explanation for the semi-wetting structure. As the surface-water potential energy well depth increases, a high-density region of water comes into existence close to the surface. This coincides with the creation of an adjacent low-density region due to van der Waals repulsion with the initial layer. As the discrepancy in density between the layers becomes greater, molecules at the interface benefit less-and-less from adopting the non-wetting structure of pointing three hydrogen bonding groups away from the surface, since the number of available hydrogen bond acceptors and donors in the neighboring region is low. This is illustrated in Figure 5.2. The emergence of the semi-wetting structure occurs in relatively high-contact-angle systems, evident starting at a contact angle as large as $\approx 130°$. This is because the high density of the initial monolayer (reaching ≈ 1.2 g/mL in this system) and the lower density of the adjacent region (reaching ≈ 0.9 g/mL in this system) work together to create a deficit of hydrogen-bonding partners for waters in the initial high-density region. In the $134°$ CA system, the density of the first layer is already 30% higher than the density of the adjacent layer. The structure of water at a hydrophobic wall thus emerges from the combination of surface-water interactions (which create the signature density profile) and the drive to maintain as many hydrogen bonds as possible at the interface (which leads interfacial water molecules to lie flat in the plane of the interface). This model also explains many features of the hydrogen-bonding profiles for the semi-wetting systems. For the $84°$ CA system, at a distance of 3.5 Å from the surface, where the first monolayer is located, the average number of hydrogen-bonded neighbours per water molecule has dropped from $n = 3.66$ in the bulk to $n \approx 3.3$. However, where the first density minimum is located 5.5 Å from the surface, the number of hydrogen-bonded neighbours is slightly higher than in the bulk, at $n \approx 3.7$. With a lower density overall in this region, we might expect to see less hydrogen bonding between molecules. The explanation is that these molecules actually have most of their hydrogen-bonding partners in adjacent higher-density regions. Features deeper into the bulk for both structures can be attributed to dipole compensation and hydrogen bonding. The geometry of the non-wetting

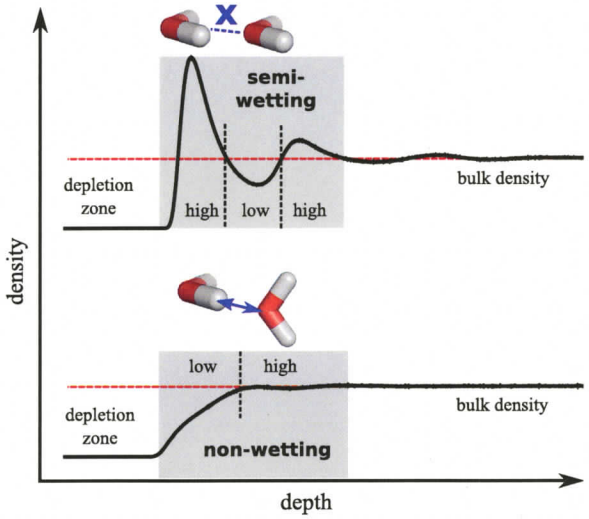

Figure 5.2: Features in the non-wetting and semi-wetting hydrophobic regimes. Interfacial molecules in the non-wetting system point three hydrogen-bonding groups toward the bulk, into a higher-density region. In the semi-wetting system, this region has a significantly lower density, forcing molecules in the first layer to maximize hydrogen-bonding opportunities with themselves. Subsequent ordering in the non-wetting regime can be attributed to dipole compensation and hydrogen bonding with the first layer.

structure at the interface leads to a net dipole field in the region of the first layer of water molecules [72]. This is partially compensated by the layer above, leading to a change in tilt angle from $\approx 60°$ at the interface to slightly more than $90°$, 2 Å away. The preference of the water molecules to adopt tilt angles around $90°$ in this region can be attributed to hydrogen bonding opportunities with the interfacial water molecules. Subsequent ordering, further from the surface, in the semi-wetting regime also depends on these two factors, although it is more complicated. After the initial layer of water, two populations of water molecules appear. These are attributed to molecules which hydrogen bond with those in the first layer. Dipole compensation and hydrogen-bonding opportunities with these two populations create two distinct populations of water molecules in each layer thereafter. Examining the tilt order parameter (Figure 3.6a), we see that semi-wetting surfaces are more strongly oriented both near the surface and in subsequent layers than non-wetting

surfaces. The same effect is observed in the twist order parameter (Figure 3.6b), which is twice as pronounced for the most-wetting surface ($S_\psi \approx 0.4$) as for the least-wetting surface ($S_\psi \approx -0.2$). This supports the observation that the semi-wetting regime comes to dominate interfacial structure as soon as a higher-density region of water forms near the surface.

5.2 Comparison with experimental water results

In recent years, visible-infrared sum-frequency generation (SFG) spectroscopy has emerged as a premier technique for studying interfacial water structure. Its popularity is mainly as a result of an extreme sensitivity to the interface, dictated by an orientation distribution of water molecules that breaks the inversion symmetry found in the bulk.

Despite their usefulness, SFG experiments face many of the same obstacles as other interface-focused experimental efforts. Although specific for regions without centrosymmetry, SFG will measure a 'blend' of signals from different regions of the interface in which centrosymmetry is broken. Also, SFG signals are dependent on several factors and require significant interpretation to be meaningful. Signal strength is dependent on the number of surface water molecules (their density in different regions of the interface), their orientation, the extent to which they are ordered, and the frequency-dependent molecular response.

Simulations can aid in interpretation of SFG spectra by providing pictures of interfacial ordering which are both complete and unambiguous. A common experiment is to tune the SFG infrared beam to the region 2800-3200 cm^{-1}, the region of O-H stretching vibrations. The O-H signal is strong and easy to detect in any form of infrared spectroscopic experiment, and O-H bonds are frequently strongly ordered at interfaces. One striking finding in these experiments, that the current study attempts to explain, is the discovery that uncoupled O-H bonds are found predominantly at non-wetting surfaces, and vanish as surfaces become more-wetting. This at first appears to be a counter-intuitive finding,

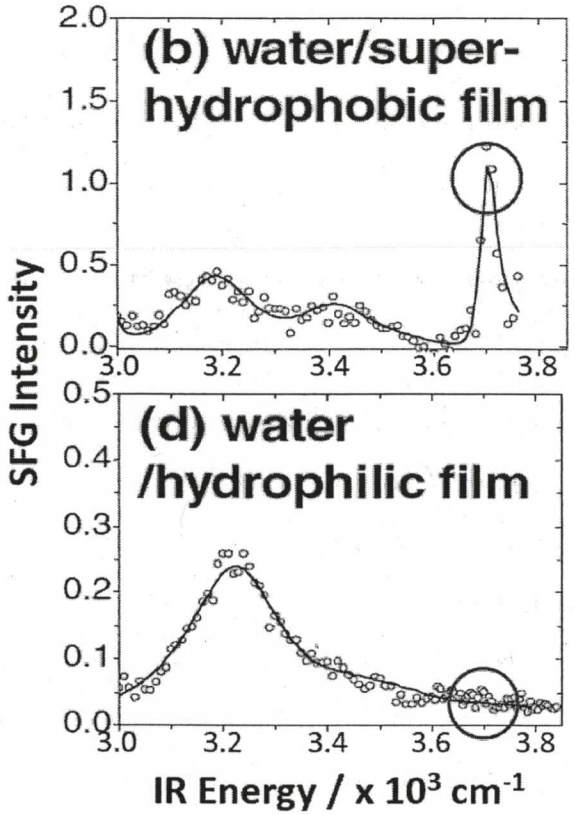

Figure 5.3: Adapted from Ref. 102. The presence of a 'naked' O - H stretching peak is clearly visible in the SFG spectrum of water at a non-wetting surface, but vanishes in the SFG spectrum of water at a semi-wetting surface.

since most wetting surfaces are at least weakly polar and would be expected to orient O-H bonds more strongly than their non-wetting counterparts. This phenomenon extends across a wide variety of surfaces of varying physical and chemical properties [101–103].

Our model of density-dependent ordering predicts that as the population of water molecules near the surface increases, there will be a gradual transition away from the non-wetting interfacial structure. This will take the form of fewer hydrogen-bonding groups projected normal to the interface, and more projected in the plane of the interface, or at an angle somewhat above or below it (since one water molecule cannot place more than two of its hydrogen-bonding groups in a plane). We observe that this transition depends

predominantly on the density profile of the interface. Polar and charged surfaces fall under the regime of wetting structures, and therefore do not direct HO bonds towards the surface. We propose that this is the reason for the absence of spectroscopic signal from uncoupled OH oscillators in SFG experiments on hydrophilic surfaces.

5.3 Extension of density-dependent ordering to Leucine adsorption

The model of density-dependent ordering proposed for interfacial water structure provides an excellent framework for interpreting leucine adsorption in our simulations. The systems used in these simulations are simple in that the surface is represented by an isotropic van der Waals potential and the adsorbate is a single amino acid. Interactions are potential well interactions between leucine and the wall, those between leucine and water, and water-water interactions. Despite the relative simplicity of the system, several different behaviours can be observed over the range of surfaces used, and dynamic behaviour is shown by the amino acid in adopting two distinctly different orientations at the surface. These behaviours arise from interactions between leucine and the water structure at the interface, which has already been shown to be highly dependent on patterns of water density.

Across all simulations, the most prominent tendency observed was for leucine's side chain, and in particular the methyl groups that terminate it, to associate strongly with the surface (Figure 4.2). This was consistent with literature [30, 32, 34, 94, 100, 104] and would be expected given the strong hydrophobicity of this part of the molecule and the nonpolar, hydrophobic nature of the surface.

As water density near the interface increased for simulations of more-wetting surfaces, it might be expected that the charged amine and carboxyl groups would directly interact with the region of high water density near the surface, but this was not observed. Any approach by the very hydrophilic amine and carboxyl groups to the solvated surface would

be opposed by hydration forces [105] arising from the conflict between the surface and solute to order the surrounding water. Effectively, any water used to solvate leucine's charged groups would be removed from the water being used to solvate the surface, and this interaction is sufficiently unfavourable that close contact between these regions of leucine and the surface does not occur.

The most non-wetting surfaces exhibit a striking feature: a strong tendency to order the leucine molecule perpendicular to the surface, which becomes stronger as the surface becomes more non-wetting, as is shown in Figure 4.4. We propose this phenomenon is due to water-leucine interactions, particularly the solvation of the amine and carboxy components.

When considering the non-wetting surfaces, there is some question as to why leucine adsorbs there at all. The attractive potential exhibited by the 156° and 151° CA surfaces is extremely weak (Figure 2.1), and shouldn't be strong enough to hold either water molecules or leucine close to the surface. The key to leucine's adsorption here lies within the surrounding aqueous environment.

The water environment near the least-wetting surfaces is dominated by a decay in density from bulk levels to zero, shown in Figure 3.2. It is beneficial for the leucine molecule to have its non-polar components in the low-density region because here they wil disrupt fewer water-water interactions than in the bulk, an interfacial version of the classic hydrophobic effect. However, it is not beneficial for leucine to have its zwitterionic groups in the low-density region, since these are charged and benefit immensely from solvation. The solution to this dilemma is for the molecule to favour a spread-out conformation and a perpendicular orientation that allows it to stretch across the low-density interface and into the bulk-density zone. The least-wetting surfaces in these simulations allow the closest approach of water molecules to the surface, as Figure 5.4 shows, since they have the shallowest repulsive potential near the surface (Figure 2.1. This causes the interface to be somewhat wider at the least-wetting surfaces (i.e. the 156° CA surface relative to the

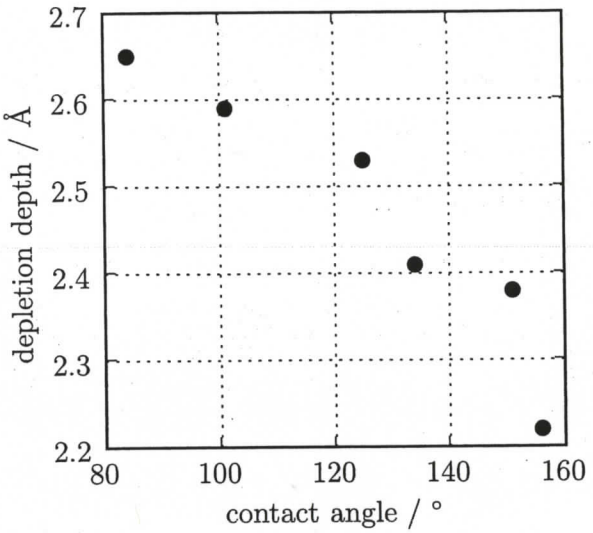

Figure 5.4: Distance from the surface where greater than 0.1% of the bulk water density is observed, plotted as a function of water contact angle.

151° CA surface). This in turn causes the orientational tendency of leucine to become more pronounced as smaller angle deviations cause the amine and carboxyl groups to be moved into the low-density interface.

There is no benefit for leucine to orient itself parallel to the surface in the least-wetting systems, and as can be seen in Figure 4.3 it adopts such an orientation only about 1% of the time. When fluctuations do cause it to orient itself roughly parallel to the surface, Figure 4.5 shows that although the methyl groups may enter the region of bulk density, the charged groups are extremely unlikely to be drawn into the interfacial region of reduced density. Figure 4.2 shows that the periods in which it may remain in this orientation last on the order of just picoseconds.

The water environment near the more-wetting surfaces is significantly different and more complicated than the non-wetting case (Figure 3.2), and leads to leucine adsorption behaviour which is also more complex. As the wetting ability of a surface increases, the tendency of leucine to adopt a laying conformation increases, illustrated by Figure 4.3. The

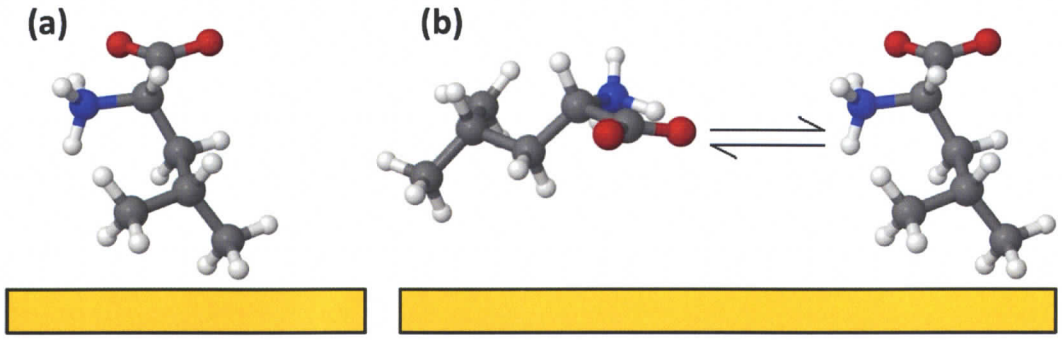

Figure 5.5: Like water, two regimes of ordering are observed for leucine adsorbed on hydrophobic surfaces. At non-wetting surfaces (a), leucine adopts a consistently perpendicular orientation to the surface. At semi-wetting surfaces (b), leucine alternates between two orientations, perpendicular and parallel to the surface.

least-wetting surfaces strongly discourage laying because it moves the amine and carboxy groups into a low-density region where they are poorly solvated. In the most-solvated systems, balance between the standing and laying states is controlled by three factors: wall potential, hydrophobic interactions, and solvation effects.

The attractive potential between the atoms of the leucine molecule and the surface itself encourages adsorption. For the more-wetting surfaces this potential is significant, particularly at the distances where the methyl groups are usually found (Figure 2.1). It is this force which stabilizes the position of the methyl groups, and leads to the tighly distributed peaks seen for the more-wetting systems in Figure 4.5.

There is also an advantageous effect to placing hydrophobic portions of the molecule in low-density regions where they will have little effect on water-water interactions. This force stabilizes the main body of the leucine molecule, including most of its side chain, which is centered in the region of low water density adjacent to the initial high-density region close to the surface. Conversely, this force destabilizes the position of the methyl groups, particularly in the standing orientation. The methyl groups appear in a region of very high water density close to the surface, where they are likely to disrupt significant

water-water interactions.

The third factor influencing adsorption is the benefit of solvating the charged amine and carboxyl groups. Solvation effects stabilize the positions of the amine and carboxy groups in the standing orientation, and destabilize them in the laying orientation. In the standing orientation, both charged groups are projected into a region of bulk or greater than bulk density adjacent to the low-density region where the body of leucine rests. In the laying orientation, however, the charged groups are forced into the low-density region where solvation may become more difficult.

The major factor supporting the laying orientation is the partial movement of the methyl groups from a high-density to low-density region of water. The main factor supporting the standing orientation is the solvation of the amine and carboxy groups. For the 84° CA surface, leucine spends about 20% of its time in the laying orientation, and for the 101 degree surface it spends about 10% of its time in this orientation, suggesting that solvation of the charged groups is the dominant effect in determining orientation, as it was for the non-wetting surfaces.

Evidence from the trajectories shown in Figure 4.2 suggests that the standing and laying orientations are distinct states and somewhat kinetically stable, as an adsorbed molecule can remain in either state for periods of more than 100 picoseconds for the 84° and 101° CA surfaces. This would not be expected if leucine continually sampled the range of available orientations. It is uncertain what causes stabilization of either orientation, but conformation may play a role. Our hypothesis is that the energy penalty associated with solvating a new orientation provides stabilization, particularly of the laying orientation. Sudden movement disrupts and scatters the water molecules involved in solvation, and the associated energy penalty provides each orientation with a degree of kinetic stability.

The application of density-dependent water ordering in this analysis can be disputed because the microenvironment surrounding leucine will be different from the wider inter-facial region, as water around leucine will structure itself to solvate the molecule. However,

this does not invalidate density-dependent ordering as a useful tool for analysis. Any solvation shell will continually be in flux, exchanging water molecules with the surrounding environment, and thus the microenvironment will depend on the macroenvironment. For example, there will be a greater penalty in free energy if leucine solvates a charged group with a molecule from a region of low-density water rather than a region of bulk density. Although density-dependent ordering does not tell the entire story of adsorption, it remains a useful tool for understanding adsorption phenomenon.

A possible contributing factor to the stability of the standing form is the relative weakness of water-water interactions in the initial high-density layer. Our own results in Figure 3.5 have shown that these water molecules are oriented in a plane parallel to the surface, and have difficulty forming complete hydrogen bonds with one another due to this orientational constraint. They also have few partners for hydrogen bonding in adjacent layers, as the initial high-density region is bordered by a corresponding low-density region in either direction. Although the methyl groups of leucine disrupt a greater number of water-water interactions by entering this layer, this may be partially offset by the relative weakness of many of these interactions.

5.4 Comparison with experimental studies of amino acid adsorption

The consensus opinion of amino acid adsorption experiments is that, except for acidic and basic amino acids, physisorption of the zwitterion driven by hydrophobic interaction with the surface is the dominant mode of reversible adsorption for amino acids [32]. The physical, reversible nature of amino acid adsorption under neutral aqueous conditions is indicated by the sensitivity of adsorption to temperature [30,93,100], and the relatively low heats of adsorption [32] and values of adsorption coefficents [34] on most surfaces. The hydrophobic nature of this interaction is indicated by its pH insensitivity [30,32,100,104] and the increasing adsorption affinity of amino acids with larger nonpolar side chains [32,

34, 94, 104]. The role of electrostatic attraction in this adsorption appears to be secondary, although it has been reported to play a role in adsorbing amino acids carrying a net charge even when these species are at very low concentrations [31, 34]. Other examples of pH sensitivity, in which adsorption affinity decreases with net charge, have been attributed to solute-solute charge interactions at the surface which prevent packing [40].

Our own results agree strongly with this view of amino acid adsorption. We observed that the interaction of the leucine's nonpolar side-chain with the solid surface and with interfacial water was the driving force of adsorption. For very non-wetting surfaces, adsorption was due to the hydrophobic effect, in which leucine's nonpolar side-chain resided in a region of low water density near the surface. For more-wetting surfaces, adsorption was promoted by wall-solute attraction as well as the hydrophobic effect, as leucine's side chain resided in a region of reduced water density adjacent to the initial high-water-density region at the interface.

The importance of hydrophobic interactions in physisorption of amino acids is so great that experiments indicate they are the driving force for adsorption even at hydrophilic surfaces such as quartz. The findings of Alladine and Nygren [106] showed that leucine, with a nonpolar side chain, had a greater affinity for polar quartz than did serine, with a polar side chain. Results suggest that polar amino acids in general are less strongly bound to a variety of surfaces than amino acids with nonpolar side chains, in the absence of specific chemical or fully-ionic interactions [32, 34, 94].

Even more surprising is the result that nonpolar amino acids actually adsorb more strongly to some hydrophilic than hydrophobic surfaces [30, 106], suggesting that something more than the hydrophobic effect is repsonsible for adsorption. This finding has led to some conflicting claims in the literature. Alladine and Nygren [106] found that the free energy of adsorption of leucine was higher on a hydrophilic than a hydrophobic surface, but did not attempt to decompose the free energy of adsorption into its enthalpic and entropic components. They suggested the greater free energy of adsorption was an enthalpic

effect arising from electrostatic interactions between leucine and their hydrophilic surface. Gregorzyck and Carta [30] found that the free energy of adsorption for phenylalanine was higher on more hydrophilic surfaces as well, but they also determined that the heat of adsorption was lower for these surfaces. They concluded that entropic effects were responsible for phenylalanine's greater affinity for hydrophilic surfaces. According to this model, the increased tendency for adsorption at a hydrophilic interface arises from the disruption of water layers near the surface. The findings of Basiuk and Gromovoy [34], who examined the adsorption of a variety of amino acids including phenylalanine on a model hydrophobic and hydrophilic surface, dispute a significant contribution from entropy to adsorption, and posit that it is an enthalpic phenomenon.

Based on our findings and the density-dependent model of ordering, we propose in this thesis an alternate hypothesis for the stronger affinity exhibited by nonpolar amino acids for certain hydrophilic surfaces. We propose that the preference of leucine and other nonpolar amino acids for these surfaces is in fact a consequence of the hydrophobic effect, as nonpolar regions of the amino acid are placed in regions of low water density near, but not directly adjacent to, the surface. This model predicts that a layer of water will mediate the adsorption of nonpolar amino acids at hydrophilic surfaces.

Chapter 6

Conclusions

We have extended existing models of water structure at super-hydrophobic surfaces to create a general model of water ordering at solid interfaces. This model has been applied to explain the orientation of leucine adsorbed in an aqueous environment.

First, molecular dynamics simulations of water at a hydrophobic solid surface were carried out. By tuning the wettability of the surface, we were able to examine the interplay of surface-water and water-water interactions. These simulations revealed the existence of two distinct regimes. When surface-water interactions are weak, water-water interactions lead to an interfacial structure resembling the air-water interface, with molecules immediately adjacent to the surface directing a hydrogen toward the surface. When surface-water interactions are strong, we observe a structure in which water molecules prefer to lie in a plane parallel to the surface. The transition between these regimes is smooth. The non-wetting regime arises from the need of water molecules at the interface to maximize their hydrogen-bonding opportunity. As the surface-water interaction increases, so does density close to the surface. As molecules in the high-density region cannot find partners in the adjacent lower-density region, the effectiveness of the non-wetting regime is reduced. This leads to the emergence of the semi-wetting regime, in which water molecules at the interface lie flat to minimize dipolar interactions and maximize the number of partial or complete hydrogen bonds with one another. Features further into the bulk for both the non-wetting and semi-wetting regimes can be explained

by hydrogen-bonding and dipole compensation with the initial layers. A link between theory and experiment exists in the prediction that ultrahydrophobic surfaces support the idea of a non-bonded OH group, in agreement with observations from nonlinear vibrational spectroscopy.

This density-dependent model of water structure was used to explain features of leucine's adsorption at a hydrophobic surface. The surfaces were used for a further series of simulations incorporating both leucine and water. Leucine was found to adsorb to all surfaces examined; at the least-wetting surfaces, we propose that adsorption is driven by the benefit of locating the nonpolar region of leucine's side-chain in the low-density region of water near the surface. This leads to straightforward orientational behaviour, in which the amino acid is adsorbed perpendicular to the surface to keep its amine and carboxyl groups in regions of bulk water density to aid in solvation. At the most-wetting surfaces, three distinct forces were found to drive adsorption: attraction between the surface and leucine, hydrophobic effects arising from the placement of leucine's side-chain in a low-density region of water, and solvation effects. The interplay between these elements led to two stable orientations of leucine at the interface: perpendicular, and parallel to, the surface. The perpendicular orientation, which leucine adopted about 80% of the time it was adsorbed to the most-wetting surface, led to better solvation of the amine and carboxy groups, but had reduced hydrophobic attraction because of the placement of its methyl groups within the initial high-density layer of water. The parallel orientation partially removed the methyl groups from their unfavourable location but also moved the charged groups into a lower-density region of water in which solvation would be reduced. The prevalence of the perpendicular orientation decreased as surface wettability increased, presumably because the higher density of water near the surface increased the hydrophobic 'cost' of leucine placing its methyl groups there.

We found a density-dependent model of water structuring to be a simple and effective tool for studying adsorption at surfaces. The density distribution of water near a surface

can be used as a 'map' to guide interpretation of other events happening at the interface. In turn, the density distribution is strongly dependent on the nature of the surface potential, and can be mapped out independently of other species. This model may be used to study adsorption of almost any solute at the interface between water and a nonpolar surface.

References

[1] Wang, Y.; Geng, X.; Zebolsky, D. M. *Thermochim. Acta* **2002,** *397,* 13–17.

[2] Brune, B. J.; Payne, G. F.; Chaubal, M. V. *Langmuir* **1997,** *13,* 5766–5769.

[3] Kronberg, B.; Silveston, R. Trends in Colloid and Interface Science XVI. In , Vol. 123; Pullman, B., Ed.; Springer: Berlin, 1990; Chapter On the Nature and Role of Water Structuring in the Adsorption of Nonionic Surfactants on Hydrophobic Surfaces, pages 75–83.

[4] Spohr, E. *J. Mol. Liq.* **1995,** *64,* 91–100.

[5] Horinek, D.; Serr, A.; Geisler, M.; Pirzer, T.; Slotta, U.; Lud, S. Q.; Garrido, J. A.; Scheibel, T.; Hugel, T.; Netz, R. R. *PNAS* **2008,** *105,* 2842–2847.

[6] Richmond, G. L. *Chem. Rev.* **2002,** *102,* 2693–2724.

[7] Pareek, A.; Torrelles, X.; Angermund, K.; Rius, J.; Magdans, U.; Gies, H. *Langmuir* **2008,** *24,* 2459–2464.

[8] Benham, M. J.; Cook, J. C.; Li, J.-C.; Rose, D. K.; Hall, P. L.; Sarkissian, B. *Phys. Rev. B* **1989,** *39,* 633–636.

[9] Zou, S. Z.; Chen, Y. X.; Mao, B. W.; Ren, B.; Tian, Z. Q. *J. Electroanal. Chem.* **1997,** *424,* 19–24.

[10] Ong, S.; Zhao, X.; Eisenthal, K. B. *Chem. Phys. Lett.* **1992,** *191,* 327–335.

[11] Boman, F. C.; Mosorrafiti, M. J.; Gibbs, J. M.; Stepp, B. R.; Salazar, A. M.; Nguyen, S. T.; Geiger, F. M. *J. Am. Chem. Soc.* **2005,** *127,* 15368–15369.

[12] Geiger, F. M. *Ann. Rev. Phys. Chem.* **2008,** *60,* 61–83.

[13] Du, Q.; Freysz, E.; Shen, Y. R. *Phys. Rev. Lett.* **1994,** *72,* 238–241.

[14] Becraft, K. A.; Richmond, G. L. *Langmuir* **2001,** *17,* 7721–7724.

[15] Wang, J.; Buck, S.; Chen, Z. *J. Phys. Chem. B* **2002,** *106,* 11666–11672.

[16] Yang, Z.; Li, Q.; Chou, K. C. *J. Phys. Chem. C* **2009,** *113,* 8201–8205.

[17] Jena, K. C.; Hore, D. K. *J. Phys. Chem. C* **2009,** *DOI 10.1021,.*

[18] Pászti, Z.; Keszthelyi, T.; Hakkel, O.; Guczi, L. *J. Phys. Condens. Matter* **2008,** *20,* 224014.

[19] Bairoch, A. *Nucleic Acids Res.* **1999,** *28,* 304–305.

[20] Liedberg, B.; Ivarsson, B.; Lundström, I.; Salaneck, W. R. *Prog. Colloid Poly. Sci* **1985,** *70,* 67–75.

[21] Doherty, G. J.; McMahon, H. T. *Ann. Rev. Biophys.* **2007,** *37,* 65–95.

[22] Sellers, J. R. *Biochim. Biophys. Acta Mol. Cell Res.* **2000,** *1496,* 3–22.

[23] Mattu, T. S.; Pleass, R. J.; Willis, A. C.; Kilian, M.; Wormald, M. R.; Lellouch, A. C.; Rudd, P. M.; Woof, J. M.; Dwek, R. A. *J. Biol. Chem.* **1998,** *273,* 2260–2272.

[24] Kyte, J.; Doolittle, R. F. *J. Mol. Biol.* **1982,** *157,* 105–132.

[25] Vasina, E. N.; Paszek, E.; Dan V. Nicolau, J.; Nicolau, D. V. *Lab Chip* **2009,** *9,* 891-900.

[26] Zaia, D. A. M. *Amin. Aci.* **2004,** *27,* 113–118.

[27] Reeds, P. J. *J. Nutr.* **2000,** *120,* 1835S-1840S.

[28] Munsch, S.; Hartmann, M.; Ernst, S. *Chem. Commun.* **2001,** 1978–1979.

[29] Kusumoto, I. *J. Nutr.* **2001,** *131,* 2552S–2555S.

[30] Gregorczyk, D. S.; Carta, G. *Chem. Sci. Eng.* **1995,** *51,* 807–818.

[31] Krohn, J. E.; Tsapatsis, M. *Langmuir* **2005,** *21,* 8743–8750.

[32] Titus, E.; Kalkar, A. K.; Gaikar, V. G. *Coll. Surf. A* **2003,** *223,* 55–61.

[33] Vlasova, N. N.; Golovkova, L. P. *Colloid J.* **2004,** *66,* 657–662.

[34] Basiuk, V. A.; Gromovoy, T. Y. *Coll. Surf. A* **1996,** *118,* 127–140.

[35] Krohn, J. E.; Tsapatsis, M. *Langmuir* **2006,** *22,* 9350–9356.

[36] Ho, K. Y.; McKay, G.; Yeung, K. L. *Langmuir* **2003,** *19,* 3019-3024.

[37] Hartmann, M. *J. Am. Chem. Soc.* **2003,** *125,* 11283–11290.

[38] Lassen, B.; Malmsten, M. *J. Coll. Int. Sci.* **1996,** *179,* 470–477.

[39] Zimmerman, A. R.; Goyne, K. W.; Chorover, J.; Komarneni, S.; Brantley, S. L. *Org. Geochem.* **2003,** *35,* 355–375.

[40] Vinu, A.; Hossain, K. Z.; Kumar, G. S.; Ariga, K. *Carbon* **2005,** *44,* 530–536.

[41] Churchill, H.; Tend, H.; Hazen, R. M. *Amer. Mineral.* **2004,** *89,* 1048–1055.

[42] Pisarewicz, K.; Mora, D.; Pflueger, F. C.; Fields, G. B.; Mari, F. *J. Amer. Chem. Soc.* **2005,** *127,* 6207–6215.

[43] Lambert, J.-F. *Orig. Life. Evol. Biosph.* **2008,** *38,* 211–242.

[44] Bonner, W. A. *Org. Life Evo. Biosph.* **1991,** *21,* 59–111.

[45] Benetoli, L. O. B.; de Souza, C. M. D.; da Silva, K. L.; Jr., I. G. S.; de Santana, H.; Jr., A. P.; da Costa, A. C. S.; Zaia, C. T. B. V.; Zaia, D. A. M. *Orig. Life. Evol. Biosph.* **2007,** *37,* 479–493.

[46] Nocentini, M.; Gendreau, R. M.; Chittur, K. K. *Mikrochim. Acta* **1988,** *I,* 343–347.

[47] Stewart, P. S.; Costerton, J. W. *Lancet* **2001,** *358,* 135–138.

[48] Alder, B. J.; Wainwright, T. E. *J. Chem. Phys.* **1959,** *31,* 459–466.

[49] Car, R.; Parrinello, M. *Phys. Rev. Lett.* **1985,** *55,* 2471-2474.

[50] Kuhne, T. D.; Krack, M.; Mohamed, F. R.; Parrinello, M. *Phys. Rev. Lett.* **2007,** *98,* 066401.

[51] van der Spoel, D.; Lindahl, E.; Hess, B.; van Buuren, A. R.; Apol, E.; Meulenhoff, P. J.; Tieleman, D. P.; Sijbers, A. L. T. M.; Feenstra, K. A.; van Drunen, R.; Berendsen, H. J. C. *Gromacs User Manual version 4.0;* www.gromacs.org: 2005.

[52] Aziz, R. A. *J. Phys. Chem.* **1993,** *99,* 4518–4525.

[53] Image retreived from: http://en.wikipedia.org/wiki/Lennard_jones_potential on December 14, 2009.

[54] Berendsen, H. J. C.; Postma, J. P. M.; Hermans, W. F. Intermolecular Forces. In ; Pullman, B., Ed.; Reidel Publishing Company: Dordrecht, 1981; Chapter Interaction models for water in relation to protein hydration, pages 331–342.

[55] Jorgensen, W. L.; Chandrasekhar, J.; Madura, J. D.; Impey, R. W.; Klein, M. L. *J. Chem. Phys.* **1983,** *79,* 926–935.

[56] Mahoney, M. W.; Jorgensen, W. L. *J. Chem. Phys.* **2000,** *112,* 8910–8922.

[57] Berendsen, H. J. C.; Grigera, J. R.; Straatsma, T. P. *J. Phys. Chem.* **1987,** *91,* 6269-6271.

[58] Grigera, J. R.; Kalko, S. G.; Fischbarg, J. *Langumir* **1996,** *12,* 154–158.

[59] Mamatkulov, I.; Khabibullaev, P. K.; Netz, R. R. *Langmuir* **2004,** *20,* 4756-4763.

[60] Jorgensen, W. L.; Tirado-Rives, J. *Jour. Am. Chem. Soc* **1987,** *110,* 1657–1666.

[61] Jorgensen, W. L.; Maxwell, D. S.; Tirado-Rives, J. *J. Am. Chem. Soc.* **1996,** *118,* 11225–11236.

[62] van der Spoel, D.; Lindahl, E.; Hess, B.; Groenhof, G.; Mark, A. E.; Berendsen, H. J. C. *J. Comp. Chem.* **2005,** *26,* 1701–1718.

[63] Berendsen, H. J. C. Computer Simulations in Material Science. In ; Meyer, M.; Pontikis, V., Eds.; Kluwer: Dordrecht, 1991; Chapter Transport Properties Computed by linear response through weak coupling to a bath, pages 139–155.

[64] Berendsen, H. J. C.; DiNola, J. P. M.; Haak, A. *J. Chem. Phys.* **1984,** *81,* 3684–3690.

[65] Maccarini, M. *Biointerphases* **2007,** *2,* MR1–MR15.

[66] de Leeuw, N. H.; Cooper, T. G. *J. Mat. Chem.* **2002,** *93,* 93–101.

[67] Sebastien, K.; Cooke, D. J.; Spagnoli, D.; Parker, S. C. *J. Mat. Chem.* **2005,** *15,* 1454–1462.

[68] Du, Z.; de Leeuw, N. H. *Dalton Trans.* **2006,** 2623–2634.

[69] Hayward, J. A.; Haymet, A. D. J. *J. Phys. Chem.* **2001,** *114,* 3713–3726.

[70] Marry, V.; Rotenberg, B.; Turq, P. *Phys. Chem. Chem. Phys.* **2008,** *10,* 4802-4813.

[71] Raghavan, K.; Foster, K.; Motakabbir, K.; Berkowitz, M. *J Chem. Phys.* **1991,** *94,* 2110-2117.

[72] Lee, C. Y.; McCammon, J. A.; Rossky, P. J. *J. Chem. Phys.* **1984,** *80,* 4448–4455.

[73] Thomas, J. A.; McGaughey, A. J. H. *J. Chem. Phys.* **2007,** *126,* 034707.

[74] Abraham, F. F. *J. Chem. Phys.* **1978,** *68,* 3713-3716.

[75] Rao, M.; Berne, B. J.; Percus, J. K.; Kalos, M. H. *J. Chem. Phys.* **1979,** *71,* 3802–3806.

[76] Lee, S. H.; Rossky, P. J. *J. Chem. Phys.* **1994,** *100,* 3334–3345.

[77] Hautman, J.; Klein, M. L. *Phys. Rev. Lett.* **1991,** *67,* 1763–1766.

[78] Shi, B.; Dhir, V. K. *J. Chem. Phys.* **2009,** *130,* 034705.

[79] Hirvi, J. T.; Pakkanen, T. A. *J. Chem. Phys.* **2006,** *125,* 144712.

[80] Du, Q.; Superfine, R.; Freysz, E.; Shen, Y. R. *Phys. Rev. Lett.* **1993,** *70,* 2313–2316.

[81] Gan, W.; Wu, D.; Zhang, Z.; Feng, R.-r.; Wang, H.-f. *J. Chem. Phys.* **2006,** *124,* 114705.

[82] Schnitzer, C.; Baldelli, S.; Shultz, M. J. *J. Phys. Chem. B* **2000,** *104,* 585–590.

[83] Walker, D. S.; Hore, D. K.; Richmond, G. L. *J. Phys. Chem. B* **2006,** *110,* 20451–20459.

[84] Grishna, N.; Buch, V. *J. Chem. Phys.* **2004,** *120,* 5217–5225.

[85] Mezei, M.; Beveridge, D. L. *J. Chem. Phys.* **1981,** *72,* 622–632.

[86] De Santis, A.; Rocca, D. *J. Chem. Phys.* **1997,** *107,* 9559–9568.

[87] Rahman, A.; Stillinger, F. H. *J. Chem. Phys.* **1971,** *55,* 3336–3359.

[88] Benjamin, I. *J. Chem. Phys.* **1999,** *110,* 8070–8079.

[89] Matsumoto, M. *J. Chem. Phys.* **2007,** *126,* 054503.

[90] Haynes, C. A.; Norde, W. *Coll. Surf. B.* **1994,** *2,* 517-566.

[91] Norde, W.; Zoungrana, T. *Biotechnol. Appl. Biochem.* **1998,** *28,* 133–143.

[92] Braun, R.; Sarikaya, M.; Schulten, K. *J. Biomater. Sci. Polym. Ed.* **2002,** *13,* 747–757.

[93] Deng, F.; Sun, Y.; Gao, Q.; Xu, W.; Xu, Y.; Wu, D.; Shen, W. *J. Phys. Chem. B* **2008,** *112,* 2261–2267.

[94] Ikhsan, J.; Johnson, B. B.; Wells, J. D.; Angrove, M. J. *J. Coll. Int. Sci.* **2004,** *273,* 1–5.

[95] Langel, W.; Menken, L. *Surf. Sci.* **2003,** *538,* 1–9.

[96] Luo, X.; Quian, G.; Sagui, C.; Roland, C. *J. Phys. Chem. C* **2008,** *112,* 2640–2648.

[97] Pollet, R.; Boehme, C.; Marx, D. *Org. Life Evo. Biosp.* **2006,** *36,* 363–379.

[98] Stievano, L.; Piao, L. Y.; Lopes, I.; Meng, M.; Costa, D.; Lambert, J.-F. *Eur. J. Min.* **2007,** *19,* 321–331.

[99] Schmidt, M.; Steinemann, S. G. *Fresnius J. Anal. Chem.* **1991,** *341,* 412–415.

[100] Gregorczyk, D. S.; Carta, G. *Chem. Eng. Sci.* **1995,** *51,* 819–826.

[101] Ye, S.; Nihonyanagi, S.; Uosaki, K. *Phys. Chem. Chem. Phys.* **2001,** *3,* 3463–3469.

[102] Zhang, L.; Singh, S.; Tian, C.; Shen, Y. R.; Shannon, M. A.; Brinker, C. J. *J. Chem. Phys.* **2009,** *130,* 154702.

[103] Gurau, M.; Kim, G.; Lim, S.-M.; Albertoria, F.; Fleisher, H.; Cremer, P. *Chem. Phys. Chem.* **2003,** *4,* 1231–1233.

[104] Gao, Q.; Xu, W.; Xu, Y.; Wu, D.; Sun, Y.; Deng, F.; Shen, W. *J. Phys. Chem. B* **2008,** *112,* 2261-2267.

[105] Israelachvili, J. N. *Intermolecular and Surface Forces;* Academic Press: London, 1992.

[106] Aladdine, S.; Nygren, H. *Coll. Surf. B* **1995,** *6,* 71–79.